

Towards the Industrial Exploitation of the Oxidative Dehydrogenation of Ethane over a NiO-SnO₂-based catalyst: Regime and Parametric Sensitivity analysis

Carlos Alvarado-Camacho,^{a,b} Jeroen Poissonnier,^b Joris W. Thybaut,^{b} and Carlos O. Castillo-Araiza^{a*}*

^aLaboratory of Catalytic Reactor Engineering applied to Chemical and Biological Systems. Departamento de Ingeniería de Procesos e Hidráulica. Universidad Autónoma Metropolitana-Iztapalapa, Av. San Rafael Atlixco 186, Col. Vicentina C.P. 09340, Ciudad de México, México

^bLaboratory for Chemical Technology, Ghent University, Technologiepark 125, B-9052 Ghent, Belgium.

**Corresponding authors: coca@xanum.uam.mx and Joris.Thybaut@UGent.be*

Abstract

An industrial-scale catalytic reactor for ethylene production *via* the oxidative dehydrogenation of ethane (ODH-C₂) over a highly active and selective SnO₂-NiO based catalyst is simulated using a 2D pseudo-heterogeneous reactor model (describing both the gas and solid phase and making use of effective transfer coefficients). More particularly the dominant phenomena at the micro- and the macroscale in a reactor configuration with a low tube to particle diameter ratio (d_t/d_p) are assessed. Firstly, the relevance of kinetics and transport phenomena on the reactor performance is determined. The evaluation of the corresponding characteristic times demonstrated that axial mass dispersion and axial heat conduction only exert a negligible impact on the concentration and temperature profiles obtained in the reactor. Fluid dynamics, on the other hand, must be accounted for, particularly for an accurate simulation of the profiles around the hot spot position. A sensitivity analysis allowed assessing the impact of the operating conditions on the performance of the SnO₂-NiO catalyst in the industrial-scale reactor. Temperature and concentration profiles, mainly around the hot spot, are highly sensitive to the inlet particle Reynolds number (Re_p), the coolant temperature and the inlet concentration of ethane and oxygen. Finally, a multi-parametric sensitivity analysis was used to identify the safety operating window leading to the optimal macroscopic performance of the reactor: a coolant temperature between 410 to 440°C, an inlet concentration of ethane from 2 to 4 %mol, an inlet concentration of oxygen from 10 to 14 %mol, and a Re_p from 620 to 1000. Thus, the engineering analysis led to the development of the most simplified yet comprehensive pseudo-heterogeneous model, with reduced computational costs, which can be used with confidence in future studies for designing and optimizing the studied ODH-C₂ reactor technology.

Keywords: fluid dynamics, pseudo-heterogeneous model, industrial tubular reactor with low

d_t/d_p , ethylene, mass and heat transfer.

Notation

Roman Letters

A_i	pre-exponential factor of reaction j , $\text{mmol (g}_{\text{cat}} \text{ s)}^{-1}$ or $\text{mmol (g}_{\text{cat}} \text{ s Pa)}^{-1}$
a_s	external surface to particle volume ratio, m_s^{-1}
C_i	carbon number of i
C_n	molar concentration of component n in the gas phase, kmol m_f^{-3}
C_{n0}	inlet molar concentration of component n , kmol m_f^{-3}
C_{ns}	molar concentration of component n in the solid phase, kmol m_s^{-3}
$C_{n,ss}$	molar concentration of component n in the gas phase at steady state, kmol m_f^{-3}
$C_{ns,ss}$	molar concentration of component n in the solid phase at steady state, kmol m_s^{-3}
C_{p_f}	specific heat of the fluid, $\text{kJ (kg}_f \text{ K)}^{-1}$
C_{p_s}	specific heat of the solid, $\text{kJ (kg}_s \text{ K)}^{-1}$
d_p	particle diameter, m_s
d_t	reactor diameter, m_r
D_{ez}	axial mass dispersion coefficient, $\text{m}_r^2 \text{ h}^{-1}$
D_{er}	radial mass dispersion coefficient, $\text{m}_r^2 \text{ h}^{-1}$
E_{a_j}	activation energy of reaction j , kJ mol^{-1}
F_i	molar flow rate of the component i , $\text{mmol}_i \text{ h}^{-1}$
h_g	interfacial heat transport coefficient, $\text{kJ m}_s^{-2} (\text{h K})^{-1}$
h_w	wall heat transfer coefficient, $\text{kJ m}_r^{-2} (\text{h K})^{-1}$
k_i	reaction rate coefficient, s^{-1} or $(\text{s Pa})^{-1}$
k_{er}	radial effective thermal conductivity, $\text{kJ (m}_r \text{ h K)}^{-1}$
k_{ez}	axial effective thermal conductivity, $\text{kJ (m}_r \text{ h K)}^{-1}$
k_g	interfacial mass transfer coefficient, $\text{m}_f^3 \text{ m}_s^{-2} \text{ h}^{-1}$
K_i	adsorption equilibrium coefficient for component i , Pa^{-1}
L	reactor length, m_r
N_T	total site concentration, $\text{mmol g}_{\text{cat}}^{-1}$
p_i	partial pressure of the component i , Pa
p_{tot}	total pressure, atm
S_i	selectivity of component i ,
t	time, h
T	temperature, K
T_0	inlet temperature, K

T_b	coolant temperature, K
T_s	solid temperature, K
$T_{s,ss}$	steady state solid temperature, K
T_{ss}	steady state fluid temperature, K
U_o	superficial velocity, $m_f^3 m_r^{-2} h^{-1}$
v_z	interstitial velocity, $m_r^3 h^{-1}$
W	catalyst mass, g_{cat}
w_j	weight factor corresponding to the response j
X_i	conversion of component i,
Y_i	yield of component i,
z	axial position, m_r

Greek Letters

ε	void fraction, $m_f^3 m_r^{-3}$
θ_i	coverage fraction of component i
ρ_b	bed density, $kg_{cat} m_r^{-3}$
ρ_f	fluid density, $kg_f m_f^{-3}$

Subscripts

cat	catalyst
eff	effective
f	fluid
g	gas
i	component i
n	component n

1. Introduction

Ethane oxidative dehydrogenation (ODH-C₂) is nowadays a recognized alternative reaction concept for producing ethylene from ethane¹. Several publications²⁻⁸, including those from our research group⁹⁻¹¹, have proven the competitiveness of ODH-C₂ in comparison with the traditional ethylene production process, i.e., naphtha steam cracking. Despite that ODH-C₂ overcomes the main drawbacks of steam cracking, such as the high energy consumption and CO_x production⁶, two challenges remain for its industrial application: firstly, the development of a highly active and selective catalyst, and secondly, the design of an industrial reactor where the catalyst can reach its best performance.

Regarding the development of an ODH-C₂ catalyst, SnO₂-NiO based formulations^{3,4,12,13}, along with multi-metallic MoVNbTeO based materials^{7,8,14-16}, have been identified as the most highly active and selective catalysts. SnO₂-NiO presents several advantages^{3,4,12,13} over MoVNbTeO, including its easy, quick, less energy demanding, and reproducible synthesis. Moreover, the SnO₂-NiO based material produces only a single side product (CO₂) under a wide range of operating conditions^{3,4,13}, even during dynamic catalytic evaluation in the absence of oxygen^{11,12}, which makes this mixed oxide an attractive catalyst from an engineering perspective.

Commercial exploitation of SnO₂-NiO based catalyst for ODH-C₂ correspondingly requires an industrial reactor concept and, hence, the development of a simulation model to determine its geometrical characteristics and operating conditions leading to maximum ethylene production. Concerning the technology, a wall-cooled packed bed reactor has been proposed as one of the most appropriate options for the catalytic production of ethylene via ODH-C₂

^{9,17,26,18–25}. Nevertheless, to the best of our knowledge, the development of a comprehensive model by following detailed engineering simulations is still missing for this reactor technology. Moreover, although the promising catalytic performance ^{3,11–13} of the SnO₂-NiO based catalyst has been identified at the laboratory scale, a model for describing its industrial-scale performance has not been reported yet.

The challenges in the modelling of a wall-cooled packed bed reactor for ODH-C₂ are situated in its geometrical complexity due to the specific thermal effects taking place along the bed. In addition to the exothermicity of the desired reaction, the undesired complete oxidation produces even more heat and a unique interplay of phenomena is involved in the heat removal from the catalyst particles to the coolant at the external side of the tube. The use of both a tube-to-particle diameter ratio (d_t/d_p) lower than 10 and nonporous catalyst pellets have favoured the macroscopic performance of the reactor by promoting the fast removal of the heat generated by the selective production of ethylene ($-\Delta H_r > 105$ kJ/mol) and, particularly, by total oxidation reactions ($-\Delta H_r > 1320$ kJ/mol) leading to the formation of CO₂. This heat removal is critical for a safe industrial operation of the reactor as the magnitude of the hot spot can be minimized and the well-known thermal runaway can be avoided, while it also results in a higher ethylene selectivity²².

Most of the pseudo-continuous models proposed ^{9,17,26,18–25} to assess the performance of the ODH-C₂ in a wall-cooled packed bed reactor either make a number of simplifications which are debatable, include kinetic parameters that lack statistical significance and physical meaning ^{17,19,20,22–24}, or neglect the impact of essential transport mechanisms on the reactor performance and, hence, on the ethane conversion and ethylene selectivity ^{17–26}. Several

authors have used pseudo-homogeneous 1D models with averaged characteristics^{17,19–22,24,26}, ignoring the local impact of the radial heat and mass transfer on the macroscopic performance of the reactor. More complex approximations, pseudo-heterogeneous 2D models (describing both the gas and solid phase and making use of effective transfer coefficients), have also been used to simulate the performance of the considered reactor configuration^{9,18,23,25}. Nevertheless, two main limitations remain: firstly, most of the models adopt plug flow hydrodynamics, hence, neglecting the impact of fluid dynamics on radial temperature and concentration profiles, and secondly, even when it is taken into account, the effect of the interstitial velocity on heat and mass transfer coefficients is not (properly) considered. In addition to all the limitations set forth, no work has reported a regime analysis, i.e., an evaluation of the characteristic times in the simulations, a sensitivity analysis of the model simulations to the transport and kinetic parameters and on the range of operating conditions where the catalyst performs optimally.

Our present work, hence, aims at filling the above-presented gap by modeling the performance of a highly active and selective SnO₂-NiO based catalyst for ethylene production from ethane ODH in an industrial -scale wall-cooled packed-bed reactor. The first step in this investigation is the development of the industrial-scale reactor model based on an accurate description of the ODH-C₂ kinetics over a SnO₂-NiO based catalyst. The local impact of transport phenomena on the reactor performance is assessed via the characteristic times of the involved phenomena, which allows the identification of the dominant transport mechanisms and, hence, the reduction of the model complexity without impacting the accuracy of the simulations. Subsequently, a parametric sensitivity analysis is applied to reduce the computational effort and to acquire a better understanding on the effect of operating conditions on the performance of the SnO₂-NiO formulation considering the

potential hot spots formation. Thereby, the effect of kinetics and transport phenomena on the conversion of ethane and selectivity towards ethylene at the reactor outlet is analyzed. Finally, the multi-parametric model is applied to identify the safety operating window where the SnO₂-NiO based catalyst exhibits its best macroscopic performance in the wall-cooled packed bed reactor with low d_t/d_p .

2. Procedures

The description of the strategy adopted in our present work for the development of a “pseudo-heterogeneous” model accounting for fluid dynamics, and the simulation and optimization of the ODH-C₂ performance over a NiO-SnO₂-based catalyst in an industrial-scale wall-cooled single-tube reactor with low d_t/d_p is organized into three main sections. Firstly, § 2.1 presents the components of the catalytic reactor model with a description of the main transport phenomena and the chemical kinetics. In addition, the mathematical model accounting for all phenomena identified in the system is proposed, such that § 2.1.1 and § 2.1.2 show the engineering approach applied to calculate the effective transport parameters involved in the reactor model and the rate equations developed to describe the intrinsic ODH-C₂ kinetics over the NiO-SnO₂-based catalyst, respectively. Subsequently, § 2.2 presents the engineering methodology proposed to analyse the relevance of the individual transport phenomena and reaction steps accounted for in the mathematical model and, thus, determine the operating window where the NiO-SnO₂ catalyst meets its best performance. Finally, § 2.3 gives details on the numerical algorithms used for the solution of the reactor model.

2.1 Reactor concept and governing equations

Figure 1 schematically represents the multi-tubular wall-cooled packed-bed reactor and, more specifically, a close-up of the operation of a single-tube in this reactor, which is the study object analyzed throughout this work. The tube is packed with nonporous Al₂O₃ pellets

supporting a NiO-SnO₂ active phase. Reactions, hence, only take place on the pellet's external surface, which is in contact with the reactor bulk fluid. External cooling is applied, i.e. the tube is immersed in a molten salt bath, to control temperature excursions. A low tube-to-particle diameter ratio is used, not only to minimize the distance over which the heat needs to be transported but also to generate velocity profiles that improve micro and macroscopic heat and mass transfer along the reactor.

Ethane and oxygen, i.e. the reactants, flow over the packed bed, along with nitrogen as an inert. As soon as the reactants enter the reactor, the following phenomena occur: (i) momentum transfer, including the role of frictional resistances on the velocity field (fluid dynamics); (ii) axial heat and mass transfer by convection and dispersion through the bulk fluid phase; (iii) radial heat and mass transfer by conduction and dispersion through the bulk fluid phase; (iv) reactor-wall heat transfer encompassing the fluid phase, solid surfaces including the reactor wall, and the bath; (v) heat and mass transfer at the solid(pellet)-fluid interphase; (vi) adsorption and reaction of ethane and oxygen on the catalytic surface, and (vii) desorption of water and transport of ethylene and CO₂ from the catalytic surface of the pellet to the bulk fluid phase. This concept corresponds to a pseudo-heterogeneous 2D model, accounting for the effect of fluid dynamics on heat and mass transport, with the next set of governing equations:

Fluid phase

$$\rho_f \frac{\partial v_z}{\partial z} = 0 \quad (1)$$

Momentum (Navier-Stokes-Darcy-Forchheimer equation)

$$\rho_f \left(\frac{\partial \varepsilon v_z}{\partial t} + \varepsilon v_z \frac{\partial v_z}{\partial z} \right) = - \frac{\partial \varepsilon p_z}{\partial z} + \mu_f \left(\frac{1}{r} \frac{\partial}{\partial r} \left(r \frac{\partial \varepsilon v_z}{\partial r} \right) + \frac{\partial^2 \varepsilon v_z}{\partial z^2} \right) - \left(\frac{\mu_f}{K} \varepsilon v_z + \frac{\rho_f}{K_z} \varepsilon^2 v_z^2 \right) + \varepsilon \rho_f g_z \quad (2)$$

Mass

$$\varepsilon \frac{\partial C_n}{\partial t} + \varepsilon v_z \frac{\partial C_n}{\partial z} = \varepsilon D_r \left(\frac{\partial^2 C_n}{\partial r^2} + \frac{1}{r} \frac{\partial C_n}{\partial r} \right) + \varepsilon D_z \frac{\partial^2 C_n}{\partial z^2} + (1 - \varepsilon) k_g a_s (C_{n_s} - C_n) \quad (3)$$

Energy

$$\varepsilon \rho_f C_{pf} \frac{\partial T}{\partial t} + \varepsilon v_z \rho_f C_{pf} \frac{\partial T}{\partial z} = k_{effr} \left(\frac{\partial^2 T}{\partial r^2} + \frac{1}{r} \frac{\partial T}{\partial r} \right) + k_{effz} \frac{\partial^2 T}{\partial z^2} + (1 - \varepsilon) h_g a_s (T_s - T) \quad (4)$$

Solid phase

Mass

$$(1 - \varepsilon) \frac{\partial C_{n_s}}{\partial t} = (1 - \varepsilon) k_g a_s (C_n - C_{n_s}) + \rho_b \sum_{i=1}^5 v_{n_i} r_i \quad (5)$$

Energy

$$\rho_b C_{ps} \frac{\partial T_s}{\partial t} = (1 - \varepsilon) h_g a_s (T - T_s) + \rho_b \sum_{i=1}^5 (-\Delta H_i) r_i \quad (6)$$

The corresponding initial and boundary conditions are:

$$t = 0; \quad v_z = v_{zSS} \quad (7)$$

$$C_n = C_{nSS} \text{ and } C_{n_s} = C_{n_sSS} \quad (8)$$

$$T = T_{SS} \text{ and } T_s = T_{s,SS} \quad (9)$$

$$z = 0; \quad v_z = v_{in} \quad (10)$$

$$u_0 C_{n_0} = u_0 C_n - \varepsilon D_z \frac{\partial C_n}{\partial z} \quad (11)$$

$$u_0 \rho_f C_{pf} T_0 = u_0 \rho_f C_{pf} T - k_{effz} \frac{\partial T}{\partial z} \quad (12)$$

$$z = L; \quad \frac{\partial v_z}{\partial z} = 0, \frac{\partial C_n}{\partial z} = 0 \text{ and } \frac{\partial T}{\partial z} = 0 \quad (13)$$

$$r = 0; \quad \frac{\partial v_z}{\partial r} = 0, \frac{\partial C_n}{\partial r} = 0 \text{ and } \frac{\partial T}{\partial r} = 0 \quad (14)$$

$$r = R_t; \quad v_z = 0, \frac{\partial C_n}{\partial r} = 0 \text{ and } -k_{effr} \frac{\partial T}{\partial r} = h_w (T - T_b) \quad (15)$$

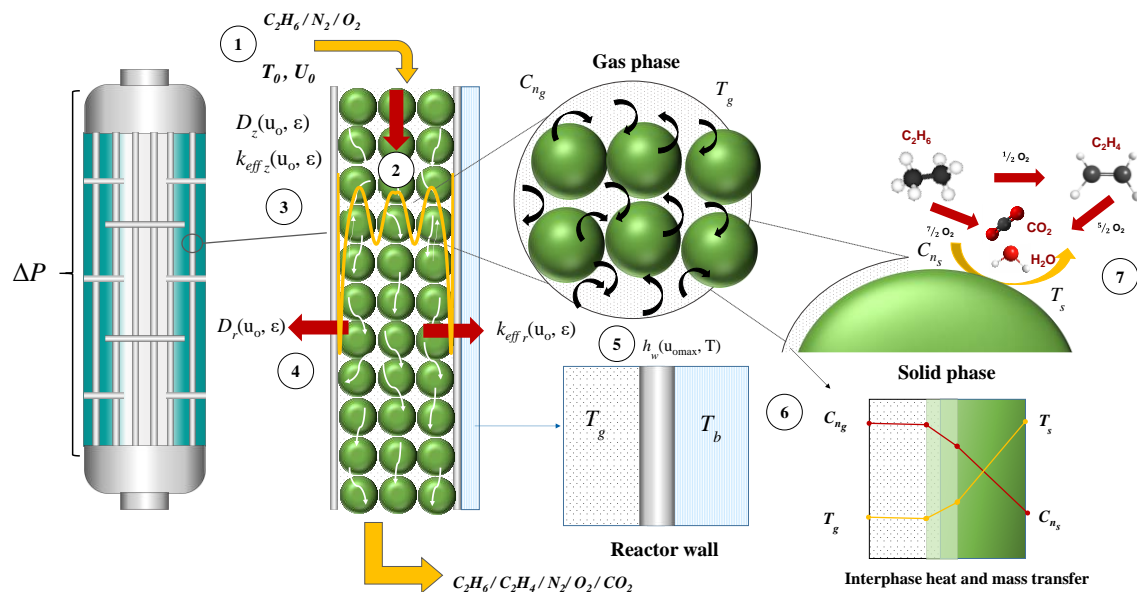


Figure 1 Schematic representation of the ODH-C₂ industrial packed-bed reactor showing the transport phenomena and kinetics included in the model.

Table 1 presents the reactor dimensions and the operating conditions employed during the simulation of the single-tube catalytic reactor, which are in line with the values of other exothermic selective oxidations already implemented in the (petro)chemical industry^{27,28}. With the aim to maintain the tube-to-particle diameter ratio below 10, particle diameters of 8.2 ($d_t/d_p=3.048$), 4.1 ($d_t/d_p=6.1$) and 2.7 mm_p ($d_t/d_p=9.15$) are considered during the simulations. The calculated bed densities (ρ_b) depending on the d_t/d_p scenario are 75.0, 82.9 and 86.7 kg_{ap} m⁻³, respectively. The feedstock composition and the coolant temperature (T_b) are based on the operating conditions employed for developing the kinetic model for the NiO-SnO₂-based material²⁹. Finally, the inlet flow rate varies in a range where the pressure drop is acceptable and leads to Re_p used during the operation of industrial wall-cooled packed bed reactors^{27,28}.

Table 1 Reactor dimensions, catalyst dimensions and operating conditions.

Reactor and catalyst dimensions		
Reactor Length	L_r [m _r]	2.6
Tube diameter	d_t [m _r]	0.025
Tube diameter to particle diameter ratio	d_t/d_p [m _r m _s ⁻¹]	3.048, 6.1, 9.15
Bed density	ρ_b [kg _{cat} m _r ⁻³]	75, 82.9, 86.7
Operating conditions		
Outlet total pressure	p_{tot} [atm]	1
Coolant temperature	T_b [°C]	360 - 480
Inlet temperature	T_0 [°C]	200
Particle Reynolds number	Re_p	200 - 1860
Flow rate	[nm ³ h ⁻¹]	2 - 6
Inlet ethane concentration	[% mol]	2 - 8
Inlet oxygen concentration	[% mol]	8 - 14

2.1.1 Transport and kinetic parameters

The characterization of all the kinetic and transport mechanisms involved during the ODH-C₂ in the wall-cooled packed-bed reactor is fundamental for the reliability of the pseudo-heterogeneous model given by the Eqs. (1) - (15). The transport parameters are determined by using well-accepted correlations reported in the literature. In § S1 of the Supporting information all equations used for determining these parameters are introduced. Table 2 presents the parameters determined for fluid dynamics, mass and heat transport. Since the development of an intrinsic kinetics model for ODH-C₂ on the SnO₂-NiO mixed oxide is imperative, the approach adopted in this work is detailed in what follows.

Table 2 Parameters range used during the modelling of the industrial-scale-wall-cooled packed bed reactor.

Transport coefficients	
$D_{ez}, m_f^2 h^{-1}$	6.7 - 92.4
$D_{er}, m_f^2 h^{-1}$	1.4 - 7.6
$k_{effz}, kJ (m_r h K)^{-1}$	16.6 - 33.1
$k_{effr}, kJ (m_r h K)^{-1}$	14.04 - 18.7
$h_w, kJ m_f^{-2} (hK)^{-1}$	1398 - 3782
$h_g, kJ m_s^{-2} (h K)^{-1}$	420 - 2104
$k_g, m_f^3 m_s^{-2} h^{-1}$	655 - 3900

2.1.2 Kinetics

The kinetic model is based on the one developed by the research group for the ODH-C₂ on the SnO₂-NiO formulation. Details concerning the synthesis method, the catalyst characterization, the experimental design, the operating conditions, and the parameter determination can be retrieved from our previous work ²⁹. Although the developed kinetic model, based on the Eley-Rideal formalism and the pseudo-steady state approach, is robust because of its mathematical and phenomenological foundation, coupling it to an industrial-scale reactor model, which is described in an equally fundamental manner, results in an overall model with a very high computation cost (i.e. the time required for a single simulation exceeds 24 h). Thus, model order reduction of the kinetic model without losing accuracy is pursued. To this end, the mechanistic steps controlling the reaction rate of the ODH-C₂ are firstly identified and, then, simplifications following the quasi-equilibrium approach are considered. § S2 in Supporting information presents this analysis, including the prediction capability of the simplified kinetic model, which is summarized as follows:

the kinetic model is based on a reaction scheme that includes parallel and consecutive reactions i.e., ethylene is produced from the oxidative dehydrogenation of ethane (r_1), and the carbon dioxide (CO_2) can be formed either directly from the combustion of ethane (r_2) or consecutively from ethylene (r_3).

$$r_1 = k_1 N_T p_{\text{C}_2\text{H}_6} \theta_0 \quad (16)$$

$$r_2 = k_2 N_T p_{\text{C}_2\text{H}_6} \theta_0 \quad (17)$$

$$r_3 = k_3 N_T p_{\text{C}_2\text{H}_4} \theta_0 \quad (18)$$

$$N_T \frac{d\theta_0}{dt} = \sum_{j=1}^N \nu_{\text{O}_j} r_{\text{O}_j} = 0 \quad (19)$$

$$\theta_{\text{H}_2\text{O}} = K_{\text{H}_2\text{O}} p_{\text{H}_2\text{O}} \theta_s \quad (20)$$

$$\theta_s + \theta_0 + \theta_{\text{H}_2\text{O}} = 1 \quad (21)$$

Here, k_j are defined as:

$$k_j^{f,r} = A_j^{f,r} \exp\left(\frac{E_{a_j}^{f,r}}{RT}\right) \quad (22)$$

where r_i , expressed by Eqs. (16)-(18), corresponds the rates of both selective and total oxidation, r_{O_j} is the adsorption-desorption rate of oxygen, k_i is the reaction rate coefficient of reaction i , N_T is the total site concentration, p_n is the partial pressure of the reactant n , $K_{\text{H}_2\text{O}}$ is the water adsorption equilibrium coefficient, θ_n is the fraction coverage of water and oxygen, θ_s is the fraction of free active sites and N_T is the total concentration of active sites.

Table 3 presents the kinetic parameters values.

Table 3 Reaction mechanism and kinetic parameters ²⁹.

Reaction Step	ΔS_n^o	ΔH_n^o	$K_n^{440^\circ\text{C}}$
	[J (mol K) ⁻¹]	[kJ mol ⁻¹]	[Pa ⁻¹]
A $\text{O}_{2(\text{g})} + 2^* \rightleftharpoons 2 \text{O}^*$	-85.6	85.7	6.37×10^{-4}
E $\text{H}_2\text{O}^* \rightleftharpoons \text{H}_2\text{O}_{(\text{g})} + ^*$	-108.7	99.7	4.21×10^{-4}
	$A_j N_T$	E_{a_j}	$k_i^{440^\circ\text{C}}$
	[mmol (g _{cat} Pa s) ⁻¹]	[KJ mol ⁻¹]	[Pa s ⁻¹]
1 $\text{C}_2\text{H}_6_{(\text{g})} + \text{O}^* \xrightarrow{\quad} \text{C}_2\text{H}_4_{(\text{g})} + \text{H}_2\text{O}^*$	9.20×10^2	66.0	1.34×10^{-2}
2 $\text{C}_2\text{H}_6_{(\text{g})} + \text{O}^* \xrightarrow{\quad} \dots \xrightarrow{+60^*} 2 \text{CO}_{2(\text{g})} + 3 \text{H}_2\text{O}^* + 4^*$	6.39×10^3	80.0	8.82×10^{-3}
3 $\text{C}_2\text{H}_4_{(\text{g})} + \text{O}^* \xrightarrow{\quad} \dots \xrightarrow{+50^*} 2 \text{CO}_{2(\text{g})} + 2 \text{H}_2\text{O}^* + 4^*$	5.53×10^3	82.0	5.45×10^{-3}

2.2 Industrial-scale modelling analysis

The simulation strategy followed three steps to confidently elucidate the performance of the SnO₂-NiO catalyst in an industrial wall-cooled packed bed reactor. Firstly, the pseudo-heterogeneity is validated by identifying the controlling mechanisms involved in the operation of the industrial reactor. An analysis of the characteristic times is performed to identify the relevant transport mechanisms in the reactor model. This analysis allows the identification of those terms that must be included in and those that can be omitted from the pseudo-heterogeneous model to guarantee, respectively not to lose its simulation accuracy. In this sense, the fluid dynamics, heat and mass transport governing equations are rearranged in terms of characteristic times, as presented in § S3 of the Supporting Information. Table 4 shows the characteristic times for the transport mechanisms involved in the wall-cooled packed bed reactor.

Table 4 Definition of the characteristic times of transport phenomena.

Mass characteristic times		Heat characteristic times	
Radial dispersion	$\tau_{D_r} = \frac{R_t^2}{D_r}$	Radial conduction	$\tau_{\text{Cond}_r} = \frac{\varepsilon \rho_F C_{p_f} R_t^2}{k_{\text{eff}_r}}$
Axial dispersion	$\tau_{D_z} = \frac{L^2}{D_z}$	Axial conduction	$\tau_{\text{Cond}_z} = \frac{\varepsilon \rho_F C_{p_f} L^2}{k_{\text{eff}_z}}$
Interphase transfer	$\tau_{\text{Int}_m} = \frac{\varepsilon}{(1 - \varepsilon)} \frac{1}{k_g a_s}$	Interphase transfer	$\tau_{\text{Int}_h} = \frac{\varepsilon}{(1 - \varepsilon)} \frac{\rho_F C_{p_f}}{h_g a_s}$
Residence time	$\tau_{\text{Conv}_z} = \frac{\varepsilon L}{u_0}$	Wall transfer	$\tau_{\text{Wall}_h} = \frac{\varepsilon}{(1 - \varepsilon)} \frac{\rho_F C_{p_f}}{h_w a_s}$

Secondly, the resulting pseudo-heterogeneous model is used to assess the performance of the industrial-scale reactor in terms of its microscopic and macroscopic responses. The effect of operating conditions on velocity, temperature, concentration, and surface species profiles along the reactor is also elucidated, providing a deeper understanding of the impact of local interactions of transport mechanisms on the overall performance of the reactor. Thus, the microscopic information is connected to the overall reactor performance in terms of the ethane conversion, ethylene selectivity and yield at the reactor outlet.

Finally, the pseudo-heterogeneous model is used to perform a multi-parametric sensitivity analysis aimed at identifying the operational window where the best catalyst performance is achieved. Because of computational constraints, the statistical response surface methodology (RSM) has been selected as the basic approach for this analysis. The RSM study is applied by using the JMP 15® commercial software, in which a total of three parameters (factors) and five responses are defined to obtain the surface response curves. The factors and the responses including their respective domains are shown in [Table S1](#) of the Supporting Information.

To analyze the overall performance of the industrial-scale reactor, the conversion of ethane and oxygen are defined in terms of the inlet molar flow rates F_i^0 and the outlet molar flow rates F_i , as follows:

$$X_i = \frac{F_i^0 - F_i}{F_i^0} \times 100\% \quad (23)$$

while the yield towards a product i , referred to as Y_i , is defined as:

$$Y_i = \frac{C_i F_i}{2F_{C_2H_6}^0} \times 100\% \quad (24)$$

And, finally, the selectivity towards a product i , referred to as S_i , is defined as:

$$S_i = \frac{C_i F_i}{2(F_{C_2H_6}^0 - F_{C_2H_6})} \times 100\% \quad (25)$$

2.3 Numerical algorithms

All the models used in this work are given by a set of parabolic partial differential equations (PDEs). The model spatial coordinates are discretized according to the orthogonal collocation method (CO) by using Legendre polynomials³⁰. The resulting set of ordinary differential equations (ODE) is solved using the Runge-Kutta-Fehlberg method³¹. Based on a mesh analysis, 20 radial and 50 axial collocation points were selected during the simulations. The algorithms were implemented in Fortran and executed in the Visual Studio 2015 interface. The simulations were performed by using two Intel XEON E5 2640 V3 processors at 2.60 GHz with 8 cores and 224 GB RAM.

3. Results and discussion

3.1 Regime analysis

Industrial-scale catalytic reactor simulations for the ODH-C₂ have frequently ignored ‘regime analyses’^{9,17,26,18–25}, such that the corresponding reactor models do not always account for all phenomena that are potentially relevant for design purposes^{17,19–22,24,26}. Thus, to ensure that all (transport) phenomena impacting on the reactor performance are included in the model

and the ODH-C₂ performance is accurately simulated at the lowest possible computational cost, a regime analysis is performed. This includes determining the characteristic time of every phenomenon involved in the reactor operation, which will provide insights on the phenomena that have the most significant impact when running the simulations. As can be seen in the rearranged equations presented in § S3 of the Supporting Information, all the characteristic times appear in the denominator of each of the terms. Therefore, in this particular case, the lower characteristic times (i.e., the fastest transfer mechanisms) will contribute significantly to the overall reactor performance during the simulations. While characteristic times can provide us with useful information on whether a phenomenon will contribute to the overall performance or not, they are not solely determining whether a phenomenon is kinetically relevant or not. Indeed, in the case of interfacial mass transfer also the difference in concentration between the solid phase and the gas phase critically determines the kinetic relevance of the transport, see Equation S(15).

Table 5 displays the effective mass transport characteristic times evaluated at a Re_p of 620, 1240 and 1860. The results show that in all cases, the characteristic times for mass transport follow the order $\tau_{\text{dispz}} \gg \tau_{\text{conv}} > \tau_{\text{dispr}} > \tau_{\text{intm}}$. Interfacial mass transport, occurring at the molecular scale, has the smallest characteristic time. Radial dispersion is the fastest phenomenon at the reactor scale, however, it is not fast enough to ensure homogeneity in the radial direction, in agreement with fluid dynamics calculations. On the other hand, axial dispersion, the slowest phenomenon, does not significantly affect the performance of an industrial-scale reactor.

Table 5 Effect of the fluid dynamics on the mass transfer characteristic times.

$$T_b = 440 \text{ }^\circ\text{C}, C_2H_6/O_2/N_2 = 8/8/84, d_t/d_p = 3.048 m_r m_s^{-1} \text{ at } z = 2.6 m_r.$$

Re_p	620	1240	1860
Mass transport characteristic times	[s]		
τ_{conv}	1.37×10^0	5.79×10^{-1}	3.70×10^{-1}
τ_{dispz}	1.74×10^3	7.71×10^2	4.97×10^2
τ_{dispr}	3.61×10^{-1}	1.76×10^{-1}	1.16×10^{-1}
τ_{intm}	1.41×10^{-2}	9.17×10^{-3}	7.14×10^{-3}

Equivalently, concerning heat transfer, **Table 6** presents the effective characteristic times evaluated at a Re_p of 620, 1240 and 1860. The characteristic time for axial conductive heat transfer surpasses the one for radial conduction, which, on its turn, exceeds the ones for interphase heat transfer and heat transfer through the tube wall, which have the same order of magnitude, $\tau_{condz} \gg \tau_{condr} \gg \tau_{inth} \approx \tau_{wall}$. This suggests that at the reactor scale, radial conduction and transfer through the tube wall will be the relevant phenomena to account for in the description of the heat transfer.

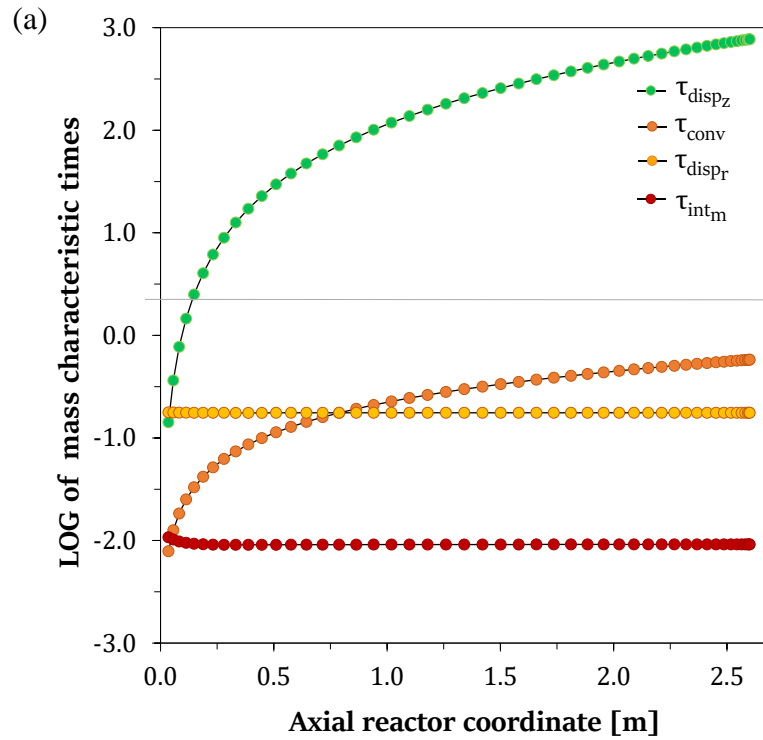
Table 6 Effect of the fluid dynamics on the heat transfer characteristic times.

$$T_b = 440 \text{ }^\circ\text{C}, C_2H_6/O_2/N_2 = 8/8/84, d_t/d_p = 3.048 m_r m_s^{-1} \text{ at } z = 2.6 m_r.$$

Re_p	620	1240	1860
Heat characteristic times	[s]		
τ_{condhr}	1.03×10^4	1.44×10^4	1.82×10^4
τ_{condhz}	3.38×10^8	4.34×10^8	5.17×10^8
τ_{inth}	1.15×10^{-2}	7.46×10^{-3}	5.81×10^{-3}
τ_{wallh}	3.10×10^{-3}	1.61×10^{-3}	1.08×10^{-3}

To complement this regime analysis, the local characteristic times are also evaluated along the wall-cooled reactor at severe operating conditions. **Figure 2** displays the logarithm of the characteristic times for transport phenomena as a function of the axial reactor coordinate. As evident from their definition (see **Table 4**), characteristic times for convection and axial dispersion vary along the axial reactor coordinate, while the other characteristic times are

constant. It can be evidenced that $\tau_{dispz} \gg \tau_{conv} > \tau_{dispr} > \tau_{intm}$ and $\tau_{condz} \gg \tau_{condr} \gg \tau_{inth} \approx \tau_{wall}$, which suggests that axial mass dispersion and heat conduction can be eliminated from the model without impacting the accuracy of the simulations.



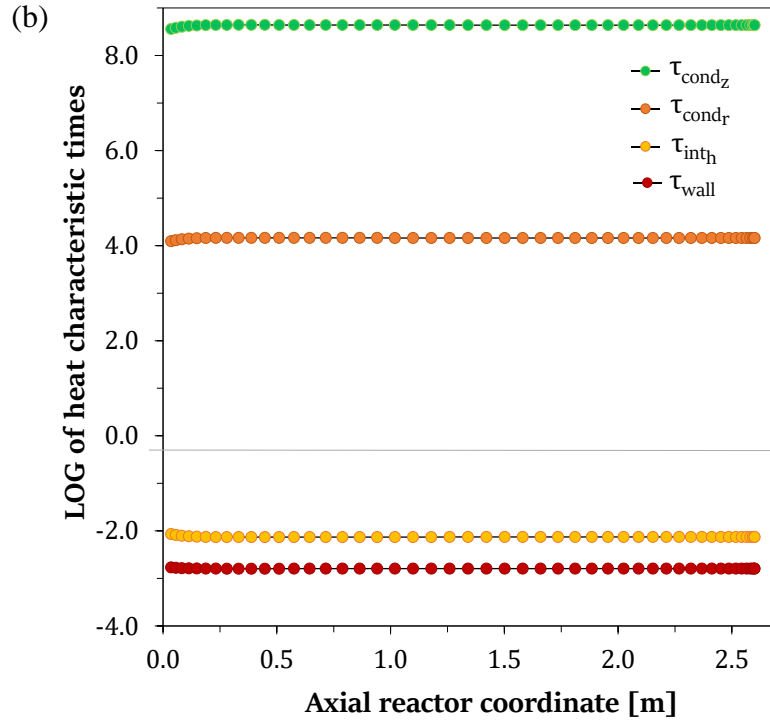
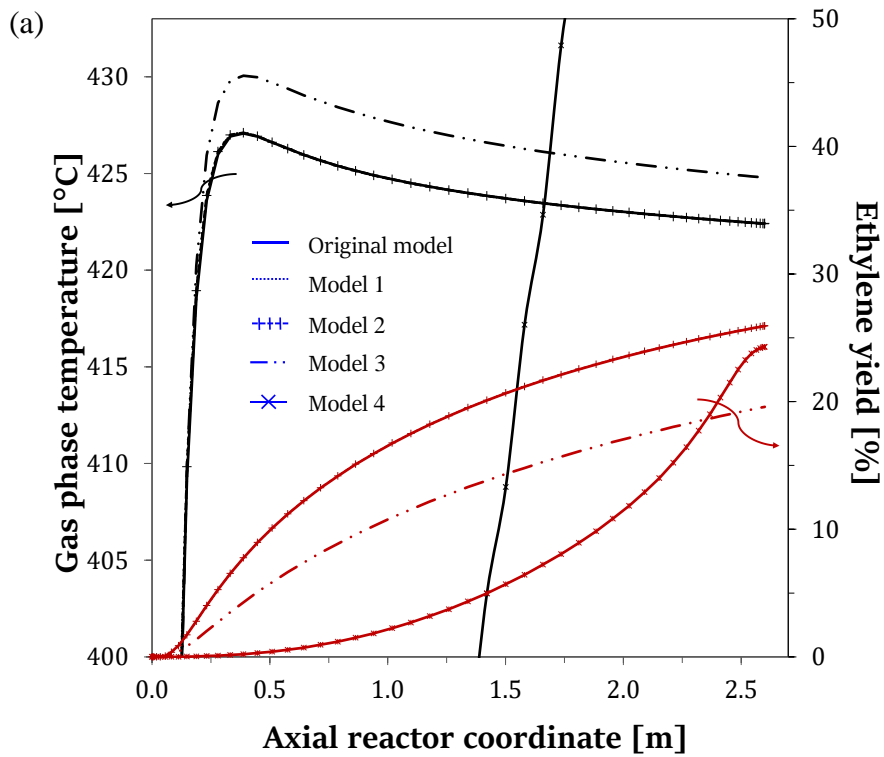


Figure 2 Logarithm of the characteristic times as a function of the axial reactor coordinate for: (a) mass transfer; and (b) heat transfer. $T_b = 440$ °C, $C_2H_6/O_2/N_2 = 8/8/84$, $d_t/d_p = 3.048 m_r m_s^{-1}$ and $Re_p = 1240$.

Once the main and relevant phenomena for the reactor operation have been identified, the pseudo-heterogeneous model, given by Eqs. (1) - (24) is applied to validate the regime analysis. Four models are derived from the original one. In § S4 of the Supporting Information the mathematical structure of each of the four models is presented. In Model 1, the term related to axial dispersion is neglected. In addition to this, Model 2 also neglects axial heat conduction. Further, in Model 3, radial mass dispersion term is then additionally neglected; while in Model 4 all terms accounting for axial and radial mass and heat transfer via dispersion and conduction, respectively, are eliminated from the model. Figure 3 displays the gas-phase temperature and the ethylene yield profiles along the axial reactor coordinate for the original model and the simplified ones. The reactor's response profiles are simulated using

a tube-to-particle diameter ratio of $3.048 \text{ m}_r \text{ m}_s^{-1}$, a particle Re_p of 1240 and two coolant temperatures, 420 and 480 °C. As expected from the regime analysis, axial dispersion and conduction can safely be omitted from the industrial-scale reactor model, without losing accuracy of the simulation, as can be seen by comparing the original model with Models 1 and Model 2, i.e., all approaches predict the same response.



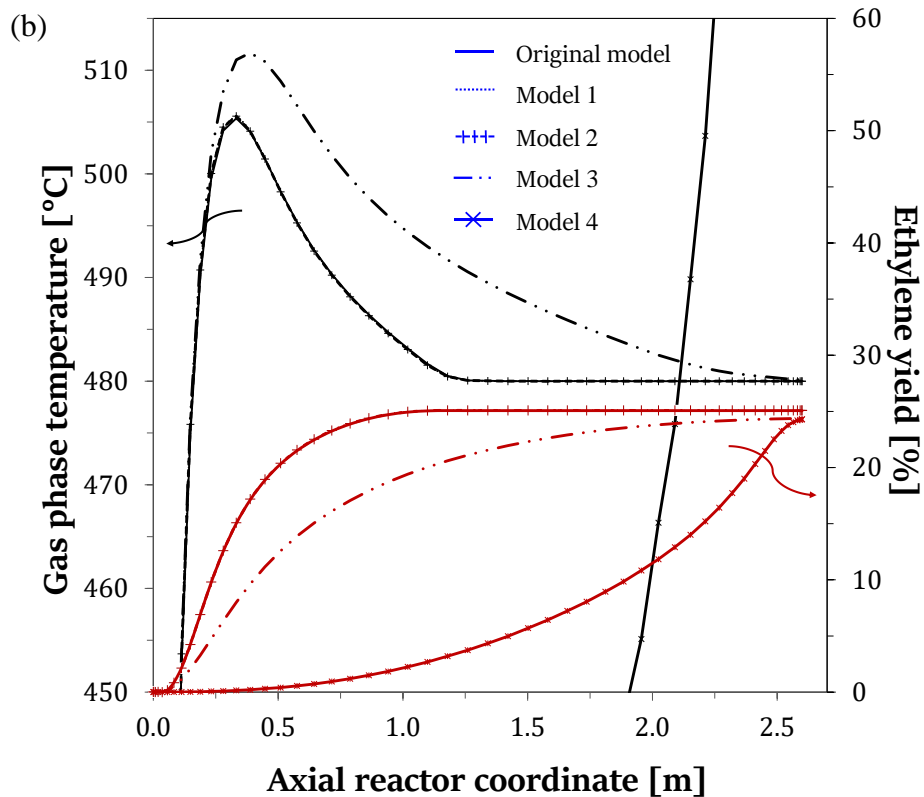


Figure 3 Gas phase temperature and ethylene yield as a function of the reactor length for: (a) $T_b=420$ °C; and (b) $T_b= 480$ °C. $C_2H_6/O_2/N_2 = 8/8/84$, $d_t/d_p = 3.048 \text{ m}_r \text{ m}_s^{-1}$, and $Re_p=1240$. The original model is described by Equations (1) - (24). In each of the simplified models an additional term compared to the previous model is omitted. Model 1: no axial dispersion; Model 2: no axial dispersion and conduction; Model 3: no axial dispersion and conduction and no radial dispersion and Model 4: no axial dispersion and conduction and no radial dispersion and conduction.

Models 3 and 4 exhibit pronounced deviations from the original model, which indicates that radial heat and mass transfer phenomena effectively need to be considered in the industrial scale packed bed reactor model. To better visualize the fit of each model to the original, [Table 7](#) show the coefficients of determination (R^2) of each model and their simulation times. For

models 1 and 2, the simulation time is reduced from 14 to 8 and 6 hours, respectively, while models 3 and 4 lead a further decrease to 4 and 2.5 hours.

Table 7 Coefficients of determination and simulation times for each model.

	Gas phase temperature		Ethylene yield		Simulation time
	R ² 420°C	R ² 480°C	R ² 420°C	R ² 480°C	[h]
Original Model	----	----	----	----	≈ 14
Model 1	0.999	0.999	0.997	0.995	≈ 8
Model 2	0.995	0.995	0.998	0.997	≈ 6
Model 3	0.737	0.964	0.825	0.641	≈ 4
Model 4	0.106	0.161	0.647	0.414	≈ 2.5

In the case of Model 1, and in agreement with the literature ³², a large L/d_p ratio (>30) and a high flow rate ($Re_p > 700$) lead to a high axial Peclet number ($Pe_{mz} > 200$), which in turn suggests that the performance of the packed bed reactor is not affected by mass dispersion in the axial direction. The transport by axial dispersion, including diffusion and back mixing, is, hence, much slower than by convection. Model 2 presumes that axial heat conduction is insignificant in contrast to dominant radial heat mechanisms. In contrast to Model 1, it is observed that for Model 3, the transport by radial dispersion plays an important role during the operation of the packed bed reactor, in agreement with the low radial Peclet number ($Pe_r = 2$ to 4). Finally, Model 4 assumes that the temperature gradients from the center of the bed to the reactor wall are “negligible”, such that the radial heat resistances are lumped into an overall heat transfer coefficient U . As can be seen in [Figure 3](#), Model 4 cannot reproduce the simulations for a highly exothermic reaction such as ODH-C₂, in a wall-cooled packed bed reactor. In fact, for Model 4, a runaway is simulated. The hot spot position and magnitude

are not predicted accurately, which is imperative for safe reactor design and operation³³. Thus, in the following, Model 2 is used during the simulation analysis as it maintains the best balance between model accuracy and computational cost.

3.2 Fluid dynamics

Figure 4 displays the interstitial axial component of the velocity and the local void fraction simulated at different d_t/d_p ratios and Re_p . Figure 4a shows the interstitial velocity along the dimensionless radial coordinate at a d_t/d_p of $3.048 \text{ m}_r \text{ m}_s^{-1}$. Velocity profiles are obtained at different Re_p , ranging from 620 to 1860, which are typical values for the industrial operation of packed bed reactors²⁷. Two zones with a high void fraction are found, i.e., one near the wall, $r^* \approx 0.97$, and another one closer to the core of the bed, $r^* \approx 0.3$. In agreement with the literature⁹, the fluid dynamic calculations indicate how those regions with larger void fractions lead to higher values of the interstitial velocity. The maximum velocities at these largest void fractions increase with the Re_p because inertial phenomena in these regions become dominant. It can be observed that the interstitial velocity is up to 2.7 times larger than the plug flow velocity (for all three Re_p) in the zone with the larger void fraction near the wall. This demonstrates the importance of taking the fluid dynamics into account, such that the impact of viscous and inertial forces caused by the solid-fluid and fluid-wall interactions can be accounted for when modelling the wall-cooled packed bed reactor with low d_t/d_p .

The velocity profiles, calculated as a function of the dimensionless radial coordinate at different d_t/d_p ratios, ranging from 3.048 to $9.15 \text{ m}_r \text{ m}_s^{-1}$, are presented in Figure 4b. Zones with high void fractions are identified along the radial coordinate for all d_t/d_p . The most pronounced one is always near the wall, $r^* \approx 0.97$, while the location of the others depends on d_t/d_p . In general, for all the d_t/d_p ratios considered, the larger the void fraction is, the higher

the interstitial velocity becomes. On the other hand, according to the literature³⁴, for d_t/d_p ratios exceeding $20 \text{ m}_r \text{ m}_s^{-1}$, a plug flow regime can be assumed.

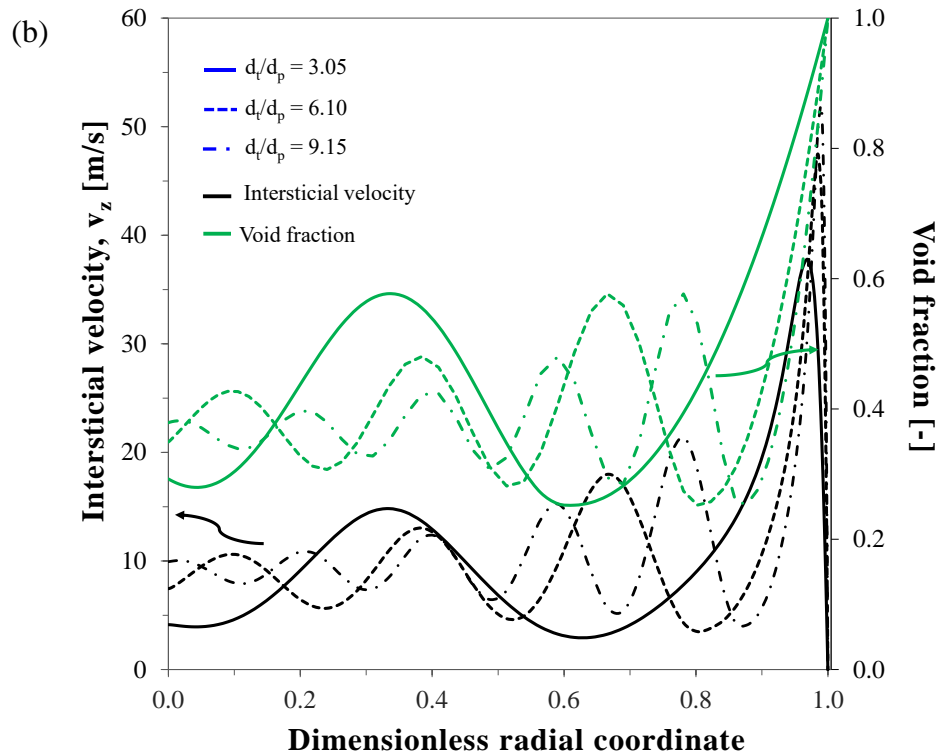
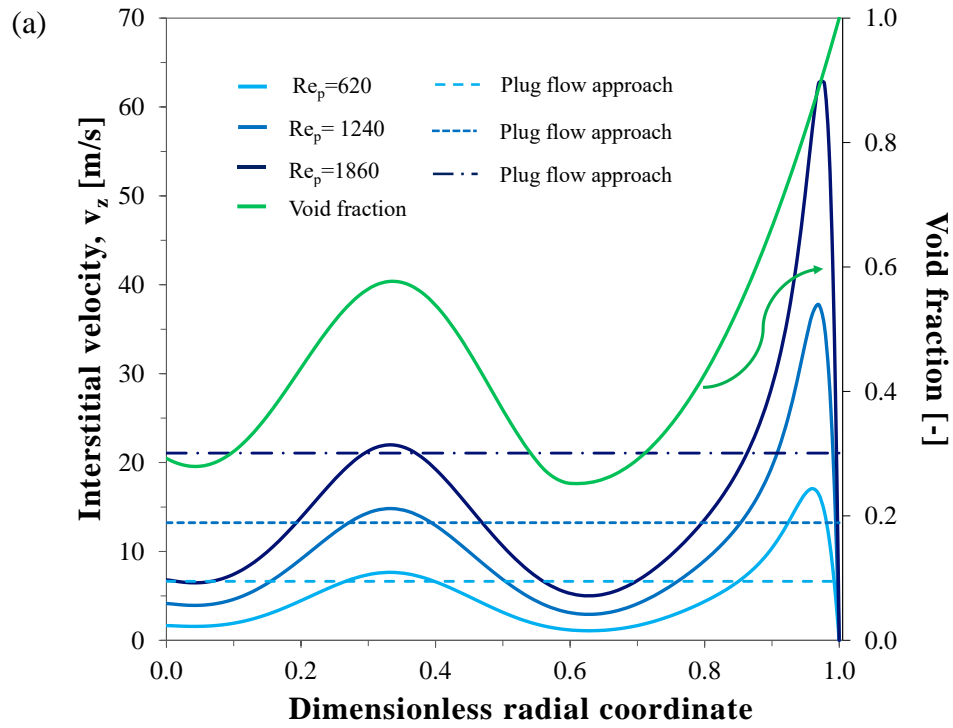
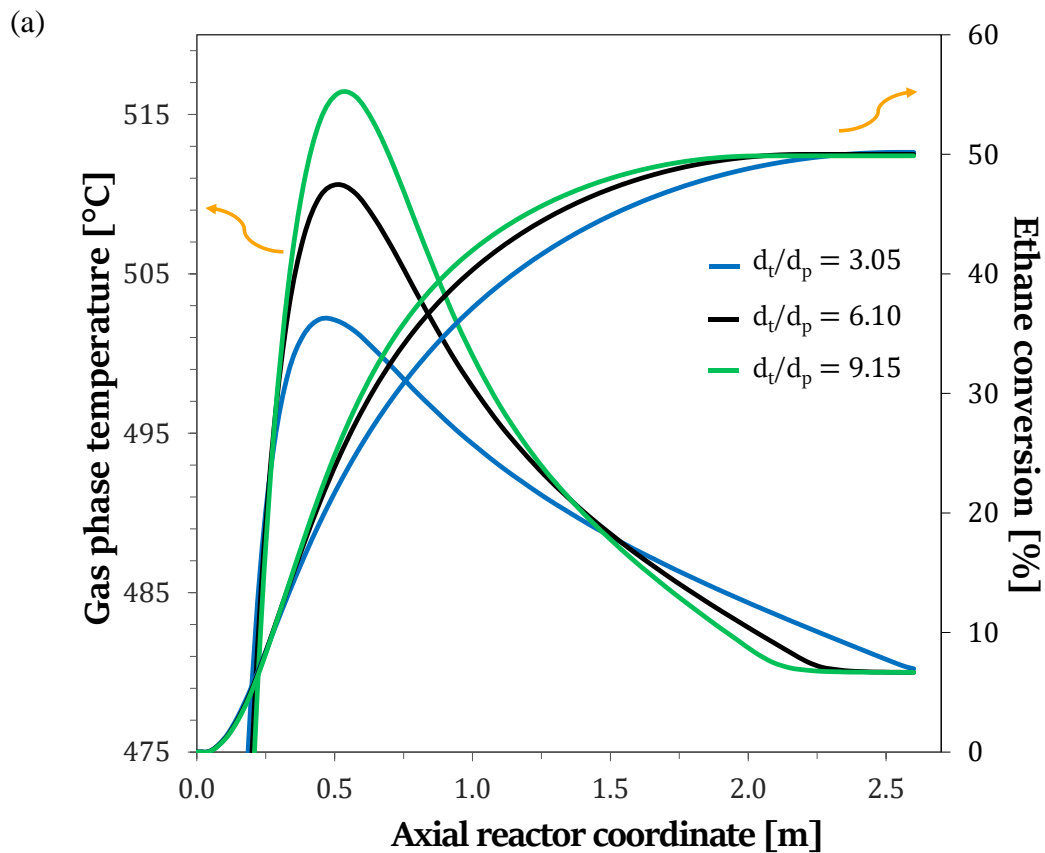


Figure 4 Void fraction and interstitial velocity profiles predicted as a function of the dimensionless radial coordinate. a) Effect of the Re_p and b) the d_t/d_p ratio on the interstitial velocity.

The effect of the fluid dynamics on the reactor performance is displayed in **Figure 5**. These simulations are performed at 480°C, by either considering fluid dynamics or following the plug flow approach. **Figure 5a** shows the gas phase temperature profile and ethane conversion as a function of the axial coordinate for different d_t/d_p ratios at a Re_p of 1240. With a coolant temperature amounting to 480 °C, a hot spot appears at an axial position of ≈ 0.5 m for all d_t/d_p . The simulated hot spot temperature increases with the d_t/d_p , e.g., at a d_t/d_p ratio amounting to $3.048 \text{ m}_r \text{ m}_s^{-1}$ a hot-spot temperature of ≈ 500 °C is obtained, while a d_t/d_p ratio of $9.15 \text{ m}_r \text{ m}_s^{-1}$ gives rise to a hot-spot temperature of ≈ 515 °C. Apart from that, although local temperature differences occur along the reactor, they only moderately affect the ethane conversion profiles and, more particularly, not at all the ethane conversion at the reactor outlet, which amounts to ≈ 50 % at all studied d_t/d_p ratios.

Figure 5b displays the axial gas and solid phase temperature profiles and ethane conversion simulated for a wall-cooled packed bed reactor considering either plug flow or the fluid dynamics approach, considering a d_t/d_p of $3.048 \text{ m}_r \text{ m}_s^{-1}$, a coolant temperature of 480 °C and a Re_p of 1240. When accounting for the fluid dynamics less pronounced hot spots are simulated, whereas when the plug flow approach is used the hot spot is simulated to be 12 °C higher. A lower ethane conversion is simulated when accounting for the velocity profiles, compared to the simulation using the plug flow approach. The maximum difference amounts to 5 % and the difference in ethane conversion at the reactor outlet is essentially negligible. The latter is attributed to this better heat dissipation caused by the higher interstitial velocity

when describing the velocity profiles explicitly. As the temperature, thus, remains lower, the simulated reaction rates are also lower and the same ethane conversion as simulated using plug flow is only obtained at a higher axial coordinate. Furthermore, as can be seen from [Figure 5b](#), temperature gradients up to 10 °C are observed between the gas and the solid phase, regardless of whether plug flow or fluid dynamics is considered during the simulations. Thus, simulations show the shortcomings of the pseudo-homogeneous model and clearly indicate the need for a pseudo-heterogeneous model coupled to fluid dynamics during the modelling of the industrial-scale packed-bed reactor.



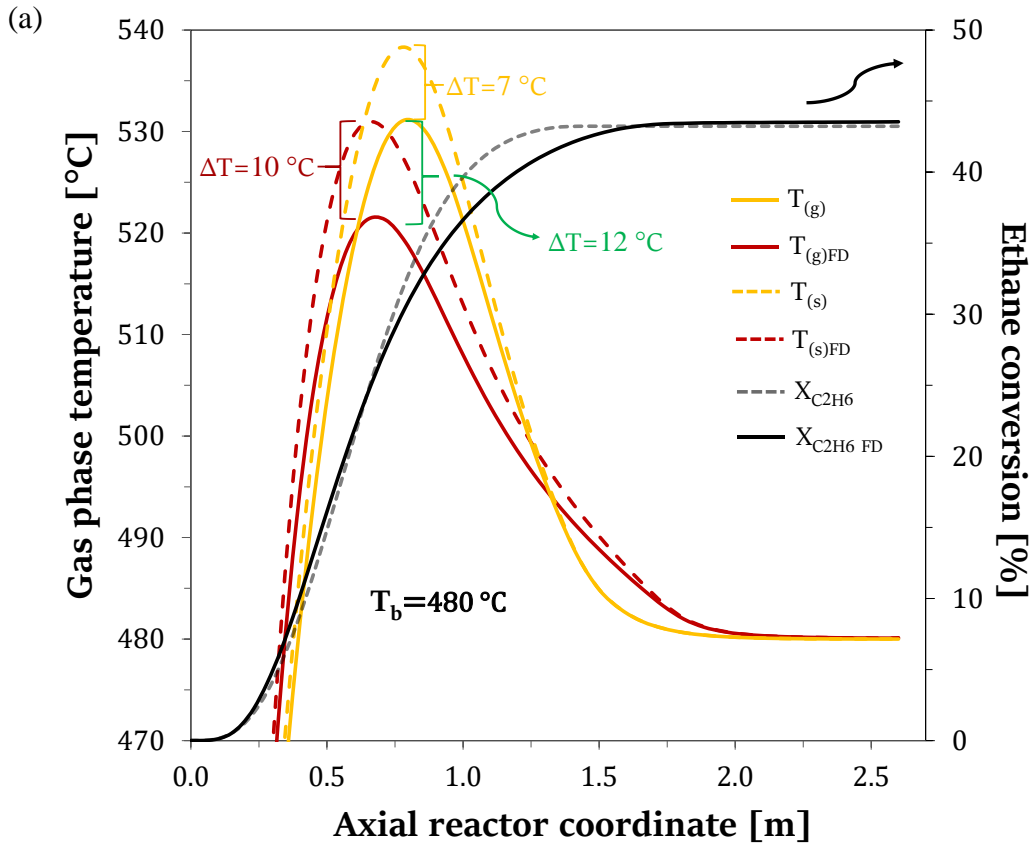


Figure 5 a) Effect of the d_t/d_p on the gas phase temperature and ethane conversion.

$T_b = 480\text{ °C}$, $C_2H_6/O_2/N_2 = 5/5/90$ and $Re_p = 1240$. (b) gas and solid phase temperature profiles at the coolant temperature of 480 °C . $T_b = 480\text{ °C}$, $C_2H_6/O_2/N_2 = 7/7/86$, $d_t/d_p = 3.048\text{ m}_r\text{ m}_s^{-1}$ and $Re_p = 1240$.

Thus, as was shown in this section, a detailed model is necessary to accurately predict packed-bed reactor performance, including the magnitude and location of hot spots. The omission of transport phenomena without prior proper analysis may result in inaccurate predictions or overestimations of hot spot temperatures, which are crucial for guaranteeing the safety during industrial scale operation.

3.3 Optimal operating window

3.3.1 Hot spot temperature

The thermal stability of the catalytic bed must be verified. To accomplish so, each promising factor combination must prevent the formation of hot spots. A hot spot is defined as an overheating beyond 20°C with respect to the set coolant temperature in at least one point of the packed-bed. Even if the hot spot by itself is not necessarily considered critical (i.e., the final temperature does not exceed 500°C which is at the onset of catalyst deactivation), it can nevertheless foment thermal instabilities within the reactor tube³⁵. In this section the formation of hot spots is analyzed as a function of the coolant temperature, the inlet molar ratio of the reactants and the inlet total flow rate.

Figure 6 shows the simulated gas phase temperature profile along the axial reactor coordinate when the coolant temperature is increased by 40°C increments from 360°C until 480 °C. For all the investigated coolant temperatures, Figure 6 indicates that the hot spots are located close to the reactor inlet, which is where the reactants (ethane and oxygen) concentrations are the highest. When comparing the gas phase profiles, an increment in coolant temperature causes an increase in the magnitude of the hot spot, which may be attributed to the more pronounced extent of deep oxidation reactions at higher temperatures while the system is not able to dissipate the generated heat. For example, a T_b of 360 °C or 400 °C causes temperature increases of about 4 °C or 10 °C, respectively, while a T_b of 440 °C or 480 °C causes pronounced hot spots with temperature increases of about 18 °C or 47 °C, respectively. Since the catalyst was calcined at 500 °C, coolant temperatures above 440 °C result in the formation of pronounced hot spots that could induce structural damage to the SnO₂-NiO based catalyst. The coolant temperature effect on the reactants conversion and ethylene yield is also

investigated in § S5 of the Supporting Information and it can be evidenced that, higher coolant temperatures result in both a higher ethane and a higher oxygen conversions. Although increases in temperature can result in higher ethylene yields, a higher T_b leads to higher CO_2 yields, which are responsible for both the formation of hot spots and the decrease in the selectivity towards ethylene. Thus for an optimal operation of the system, a trade-off between the ethane conversion and ethylene selectivity needs to be made to optimize the ethylene yield

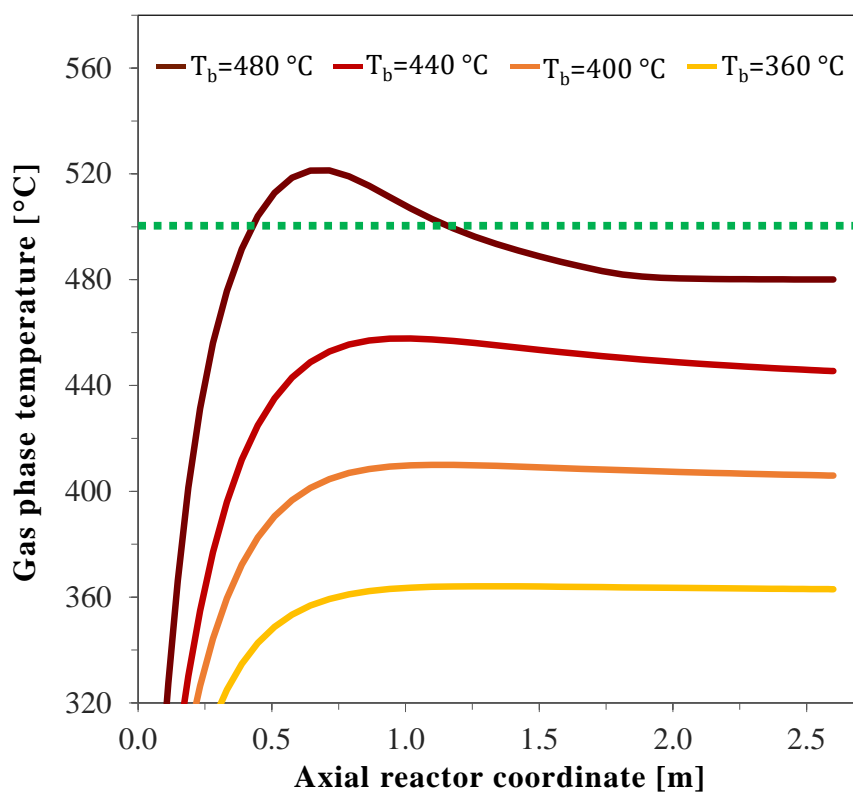
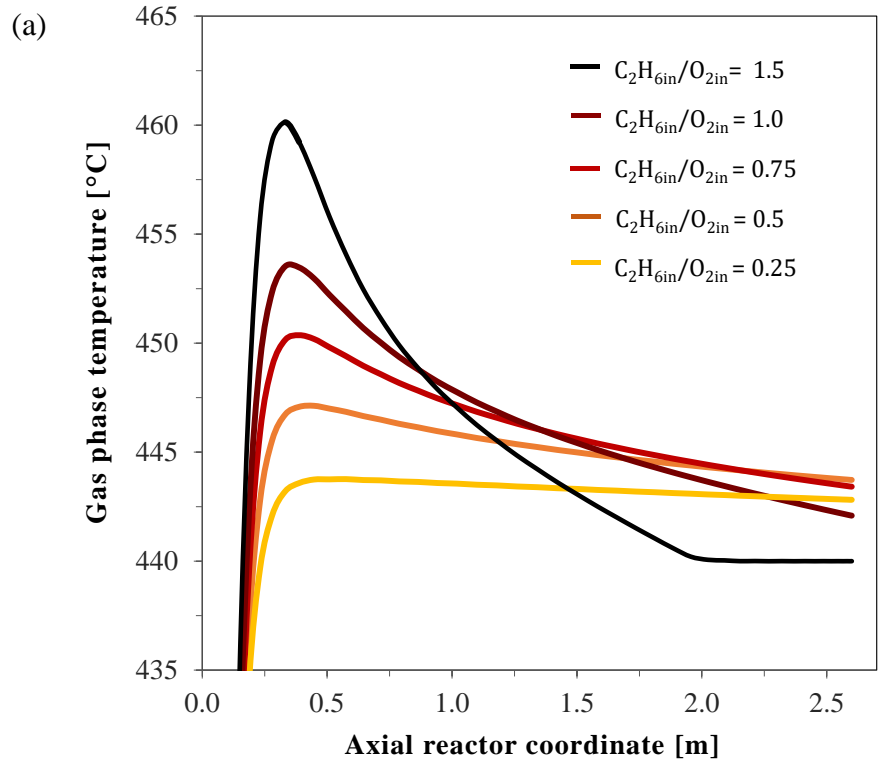
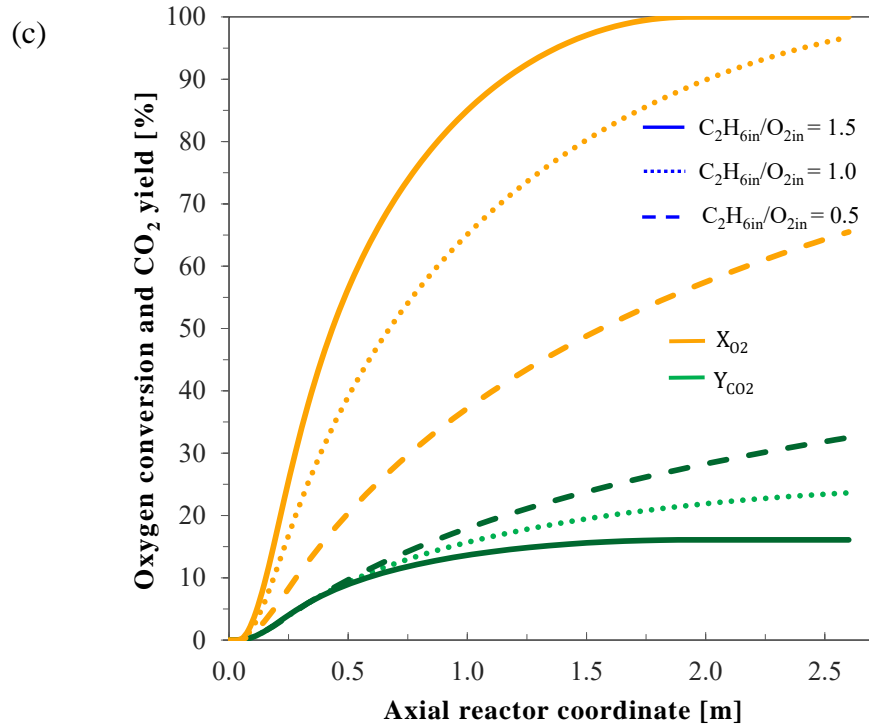
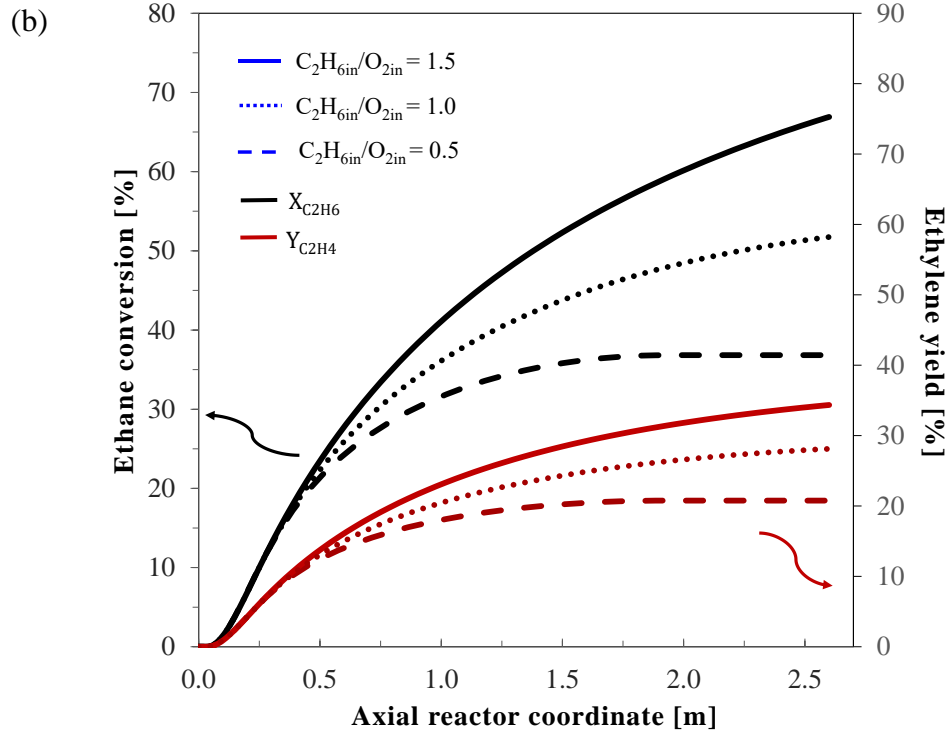


Figure 6 Effect of the coolant temperature on the gas phase temperature in the industrial-scale reactor simulations. $\text{C}_2\text{H}_6/\text{O}_2/\text{N}_2 = 7/7/86$, $d_v/d_p = 3.048 \text{ m}_r \text{ m}_s^{-1}$ and $\text{Re}_p = 1240$.

Figure 7 displays the effect of the inlet molar ratio of ethane-to-oxygen ($\text{C}_2\text{H}_{6\text{in}}/\text{O}_{2\text{in}}$) on the gas phase temperature, reactants conversion, and products yield as a function of the axial position of the reactor for a coolant temperature of 440 °C and Re_p of 1240. The inlet oxygen concentration is maintained at 8 mol% and the inlet ethane concentration varies in 5 levels

from 2 mol% to 12 mol%. For all the investigated inlet molar ratios, [Figure 7a](#) indicates that the hot spot occurs near the reactor inlet, again because the concentration of the reactants is the highest there. The magnitude of the hot spot increases with the C_2H_{6in}/O_{2in} inlet ratio, i.e., an C_2H_{6in}/O_{2in} between 0.25 to 0.75 leads to temperature increases of ca. 4 °C to 10 °C, while a C_2H_{6in}/O_{2in} from 1.0 to 1.5 results in hot spots of ca. 14 to 20 °C, respectively. [Figure 7 b-c](#) displays the effect of the C_2H_{6in}/O_{2in} on reactants conversion and products yield. A higher C_2H_{6in}/O_{2in} results in a higher oxygen conversion and a decrease in ethane conversion and products yield. The latter stems from a reduction of the ethane conversion, as the variations of the ethylene selectivity are below 5% (vide [Fig. S4](#)). Thus, although a higher C_2H_{6in}/O_{2in} results in an increase of all reaction rates, the rate of the overoxidation of hydrocarbons to CO_2 is enhanced slightly more with the increase in ethane partial pressure. [Figure 7 d](#) shows the distribution of the species adsorbed on the catalytic surface. An increase in the C_2H_{6in}/O_{2in} gives rise to a greater consumption of oxygen, and correspondingly a lower amount of oxidized sites and a higher amount of sites occupied by the water. At a lower C_2H_{6in}/O_{2in} and, hence, higher inlet oxygen concentration, more oxidized sites remain resulting in a pronounced CO_2 overoxidation .





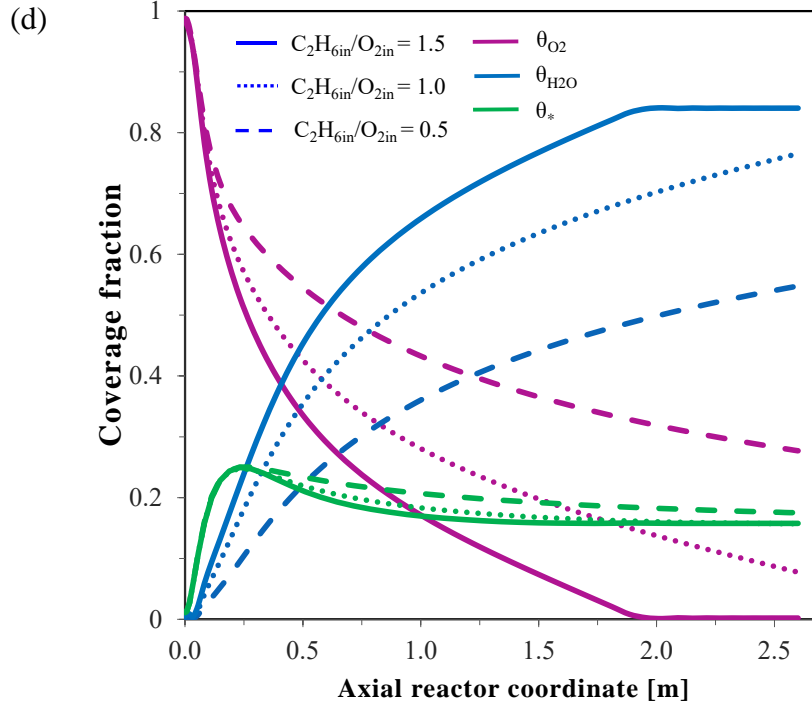


Figure 7 Effect of the ethane to oxygen inlet molar ratio on (a) the gas phase temperature, (b) ethane conversion and ethylene yield, c) oxygen conversion and CO_2 yield and d) surface coverage fractions.

$$T_b = 440 \text{ } ^\circ\text{C}, \% \text{ mol}_{O_{2in}} = 8\%, d_v/d_p = 3.048 \text{ } m_r \text{ } m_s^{-1} \text{ and } Re_p = 1240.$$

In order to better visualize the operating conditions that lead to the generation of hot spots, **Figure 8** presents the axial reactor $\Delta T(T_g - T_b)$ contours in function of the coolant temperature and the C_2H_{6in}/O_{2in} inlet ratio. The inlet oxygen concentration is maintained at 8 mol% and the inlet ethane concentration varies in 4 levels from 2 mol% to 8 mol%. From these observations, it can be concluded that the region with negligible hot spot formation can be identified when the coolant temperature does not exceed $420 \text{ } ^\circ\text{C}$ regardless of the C_2H_{6in}/O_{2in} inlet ratio. On the other hand, coolant temperatures above $440 \text{ } ^\circ\text{C}$ lead to the formation of pronounced hot spots that exceed $20 \text{ } ^\circ\text{C}$ (see **Figure 8**).

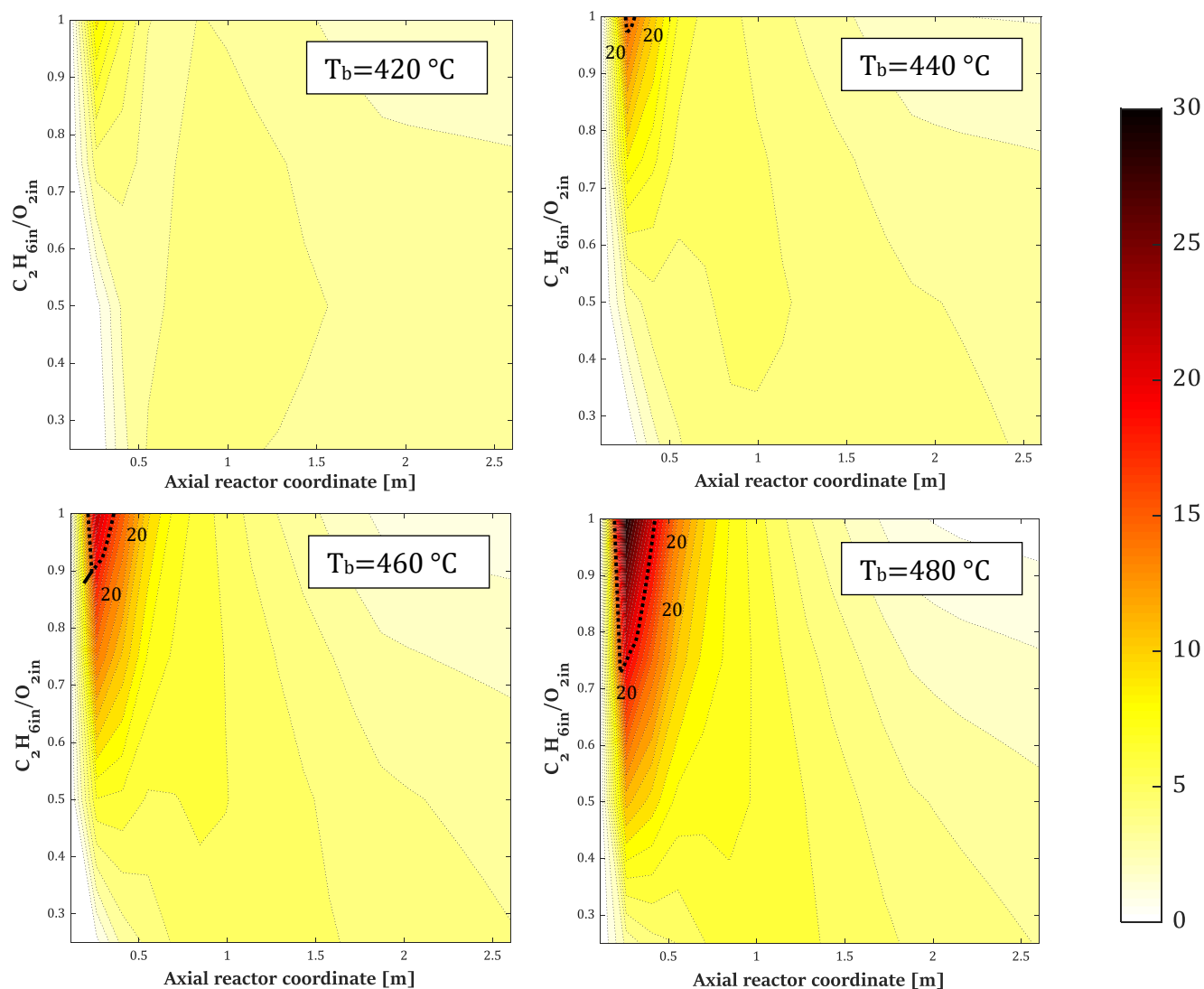
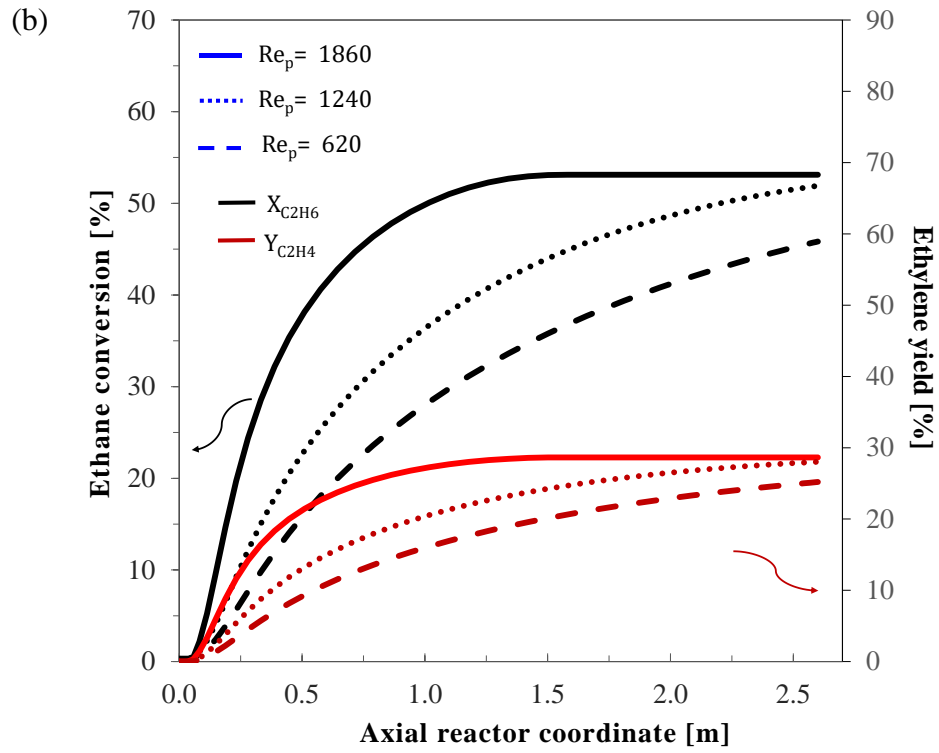
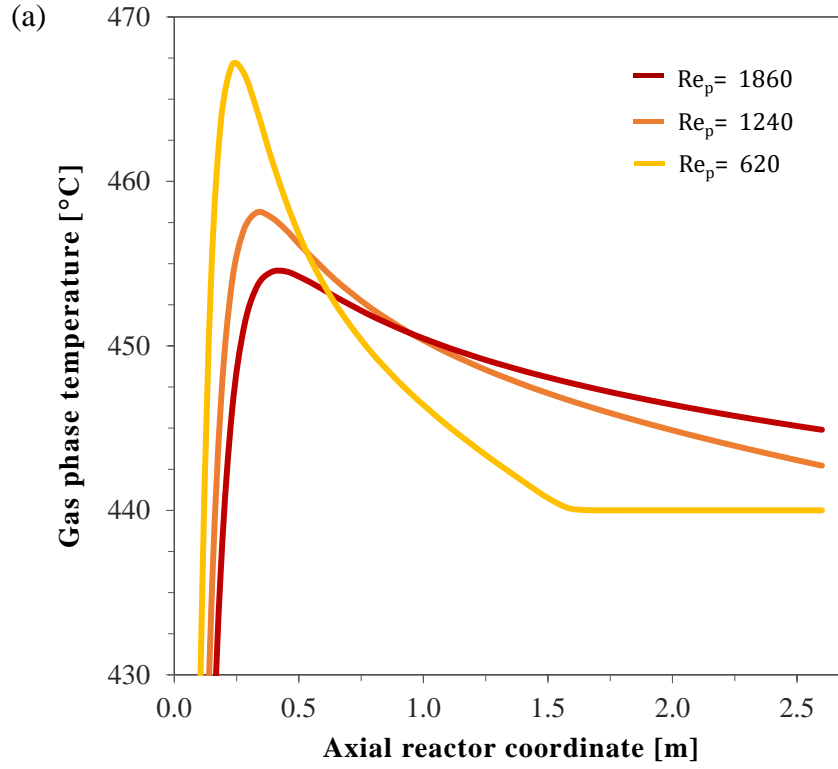


Figure 8 Axial reactor $\Delta T(T_g - T_b)$ contours in function of the coolant temperature and the C_2H_{6in}/O_{2in} inlet ratio. The critical hot spot zone (ΔT exceeding $20^\circ C$) is indicated with the dotted lines. $\% mol_{O_{2in}}=8\%$, and $d_t/d_p=3.048 m_r m_s^{-1}$ and $Re_p=1240$.

The inlet molar ratio of ethane-to-oxygen (C_2H_{6in}/O_{2in}) effect by varying the inlet oxygen concentration is also examined in § S6 of the Supporting Information. The inlet oxygen concentration is varied from 5 mol% to 14 mol% while keeping the ethane concentration fixed in the feedstock at 8 mol%. Similar trends are observed, see Figure S5 of the Supporting Information, albeit that the effects are less pronounced than when changing the ethane

concentration at a fixed oxygen concentration. The magnitude of the hot spot increases with the inlet oxygen concentration, i.e., an inlet oxygen concentration from 5 to 14 mol% leads to increments in hot spots from 10°C to 31°C, respectively.

To conclude the microscopic analysis, the effect of the inlet total flow rate was analyzed. [Figure 9](#) shows the axial profiles of the gas phase temperature, reactants conversion, and products yield along the axial reactor coordinate for a coolant temperature of 440°C and $d_i/d_p=3.048 \text{ m}_r \text{ m}_s^{-1}$ when the inlet flow rate varies from 2 to 6 Nm³ h⁻¹. As the particle Reynolds number decreases from 1240 to 620, the hot spot temperature increases from 450 °C to 465 °C, indicating that lower residence times enable better heat dissipation along the reactor (see [Figure 9a](#)). The hot spots are located close to the reactor inlet, where the most severe conditions in terms of reactant concentrations and temperature are found. As an increase in Re_p corresponds to a higher flow rate (and a higher space velocity/shorter residence time), there is a corresponding decrease in the reactants conversion and product yields (see [Figure 9 b-c](#)). This is in agreement with literature observations for some highly exothermic reactions where the total oxidation of hydrocarbons significantly competes with the selective oxidation¹⁸.



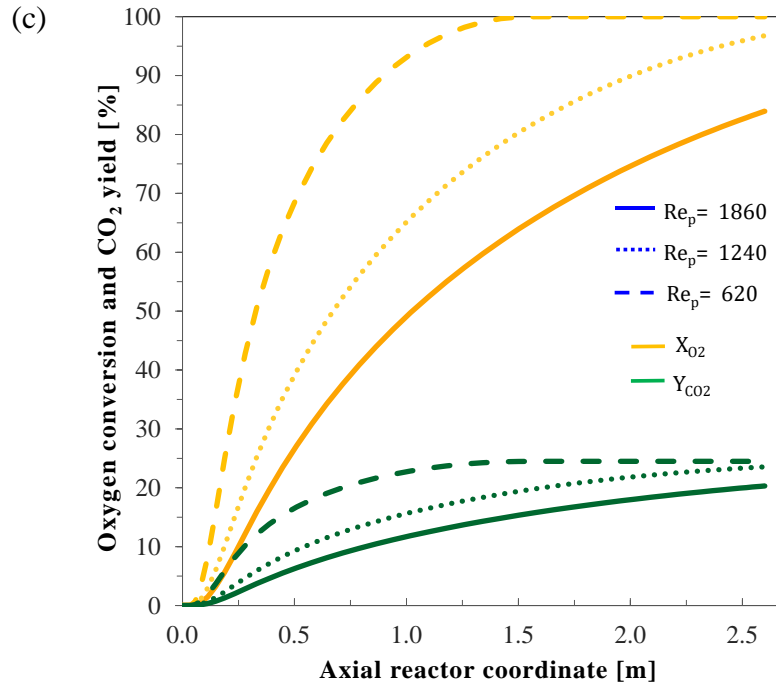
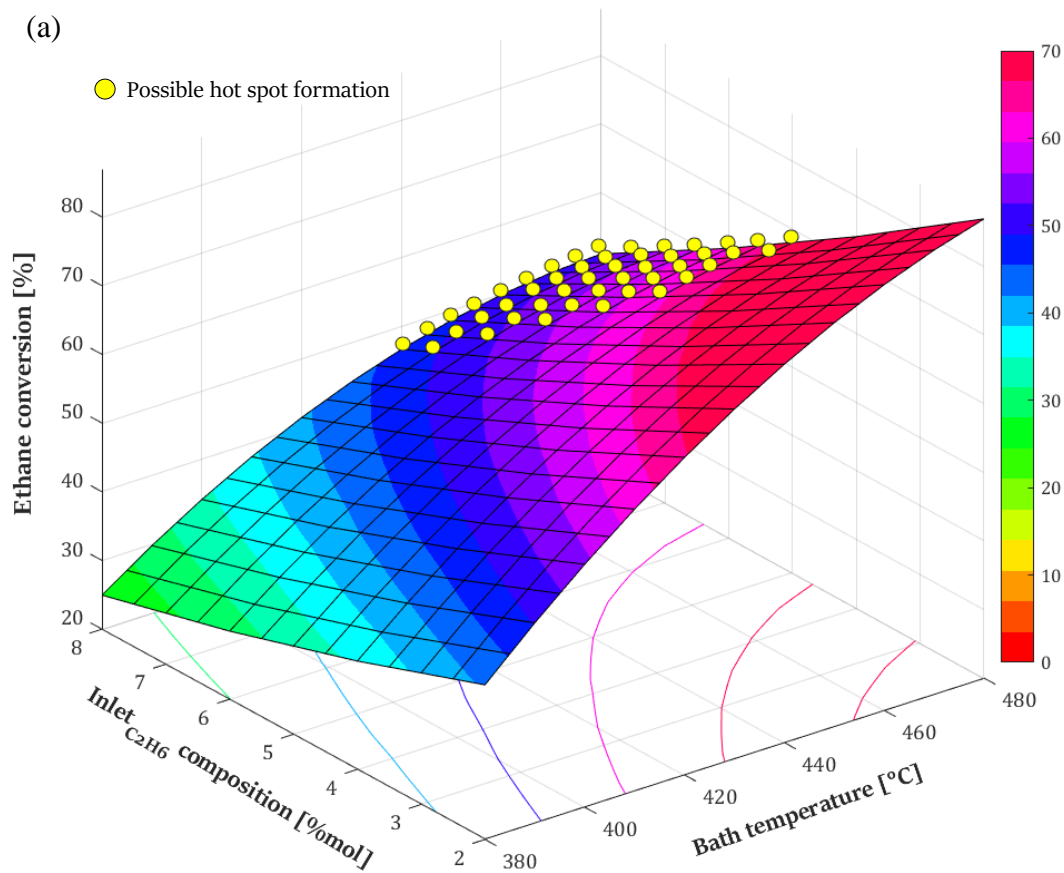


Figure 9 Effect of the Re_p on (a) gas phase temperature, (b) ethane conversion and ethylene yield, c) oxygen conversion and CO_2 yield. $T_b = 440$ °C, $C_2H_6/O_2/N_2 = 8/8/84$, and $d_t/d_p = 3.048 \text{ m}_r \text{ m}_s^{-1}$.

3.3.2 Parametric sensitivity analysis

The combined effect of all operating conditions on the overall ethane conversion and ethylene yield at the reactor outlet is assessed in view of, ultimately, identifying the operating conditions where the ODH- C_2 over the SnO_2 -NiO-based catalyst performs best without the formation of critical hot spots in a wall-cooled packed bed reactor. **Figures 10-12** display the effect of the coolant temperature (ranging from 380 to 480 °C), the feed composition (inlet ethane concentrations ranging from 2 to 8 %mol and inlet oxygen concentrations from 8 to 14 %mol), and the particle Reynolds (ranging from 620 to 1860) on the ethane conversion and the ethylene yield. Because the magnitude of the hot spots is less pronounced as the d_t/d_p ratio decreases (see [Section 3.2.1](#)), the response surfaces are made at a fixed d_t/d_p ratio of $3.048 \text{ m}_r \text{ m}_s^{-1}$.

Figure 10 displays the effect of the coolant temperature and the inlet ethane concentration on the (a) ethane conversion and the (b) ethylene yield. A positive linear relationship is obtained between the ethane conversion and both variables, which is typical for hydrocarbon oxidation. Higher ethane inlet concentrations result in lower conversions. From Figure 10 b it can be concluded that the best performance region (i.e. ethylene yields between 32 and 35 %) without hot spot formation occur when the inlet concentration of ethane ranges from 2 to 4 mol% and the coolant temperature varies between 410 and 450 °C. Coolant temperatures exceeding 450 °C and inlet concentration of ethane up to 5%mol result in a CO₂ selectivity above 55% (not shown).



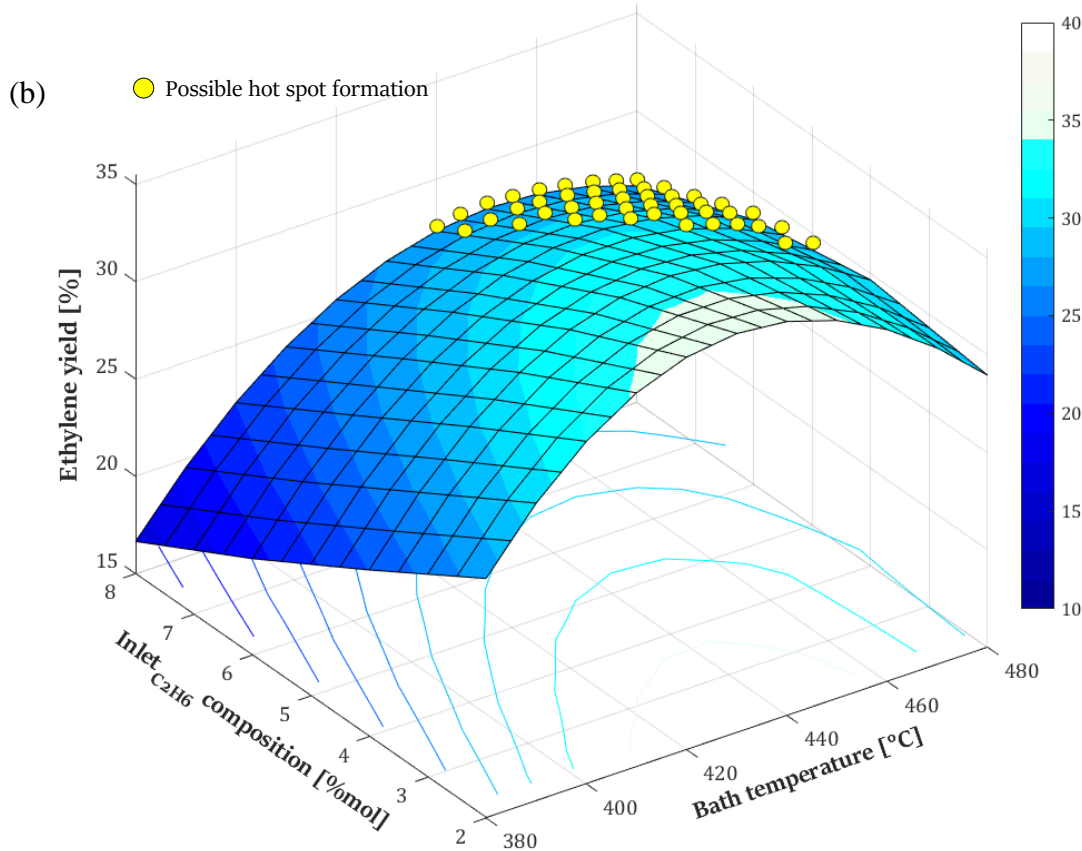
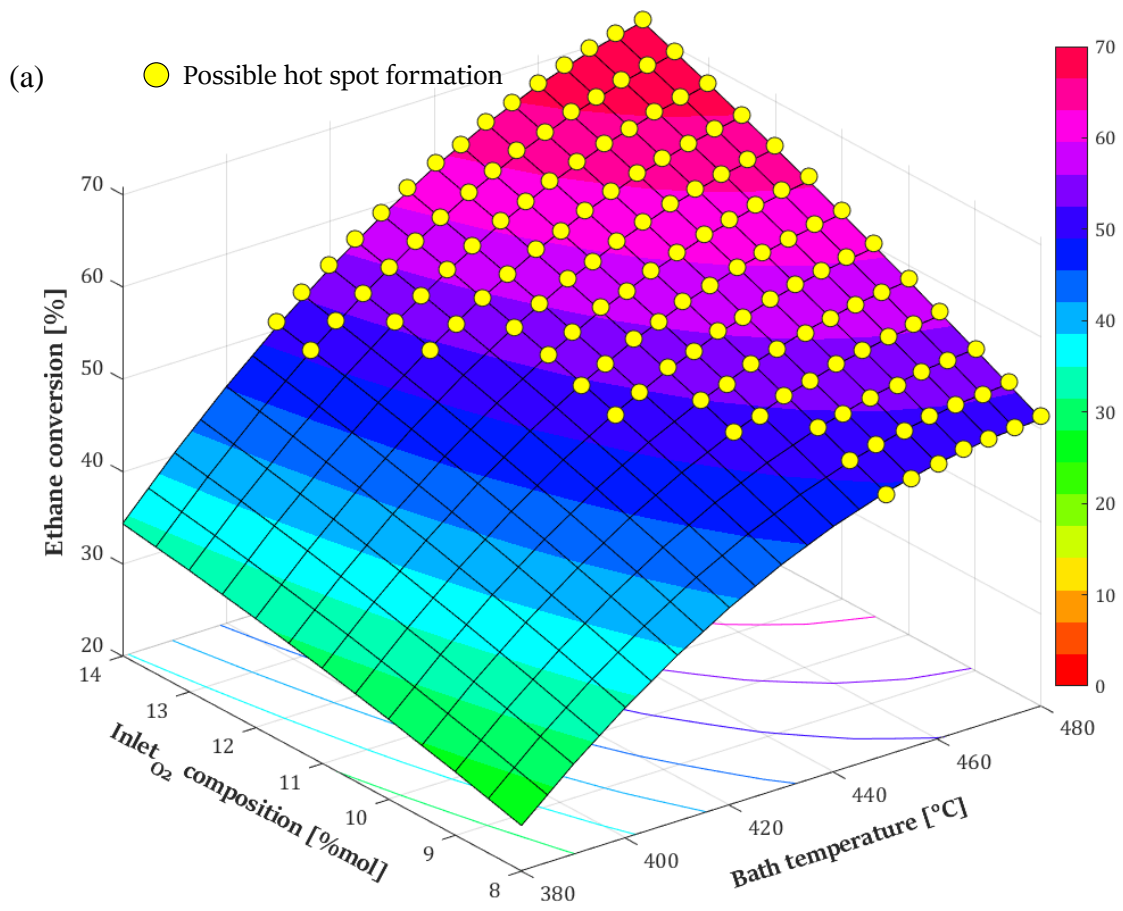


Figure 10 Effect of the coolant temperature and inlet ethane composition on the a) ethane conversion and b) ethylene yield at the reactor outlet. % mol_{O₂in}=8%, and $d_i/d_p=3.048 m_r m_s^{-1}$ and $Re_p=1240$.

Figure 11 depicts the impact of the coolant temperature and oxygen inlet fraction on the ethane conversion and ethylene yield. Increasing the oxygen inlet fraction from 8% to 14% mol results in a (pronounced) increase in ethane conversion, which stems from the correspondingly higher concentration of oxidized sites on the catalyst surface, which promotes oxidation. Figure 11b shows that in the zone where no hot spots occur a similar trend exists for the ethylene yield as a function of the coolant temperature and the inlet oxygen concentration. In a zone that avoids the formation of pronounced hot spots, ethylene yields between 29 to 31% can be achieved when the inlet oxygen molar fraction ranges from 9 to 12 mol% and at the coolant temperatures between 410 and 440 °C.



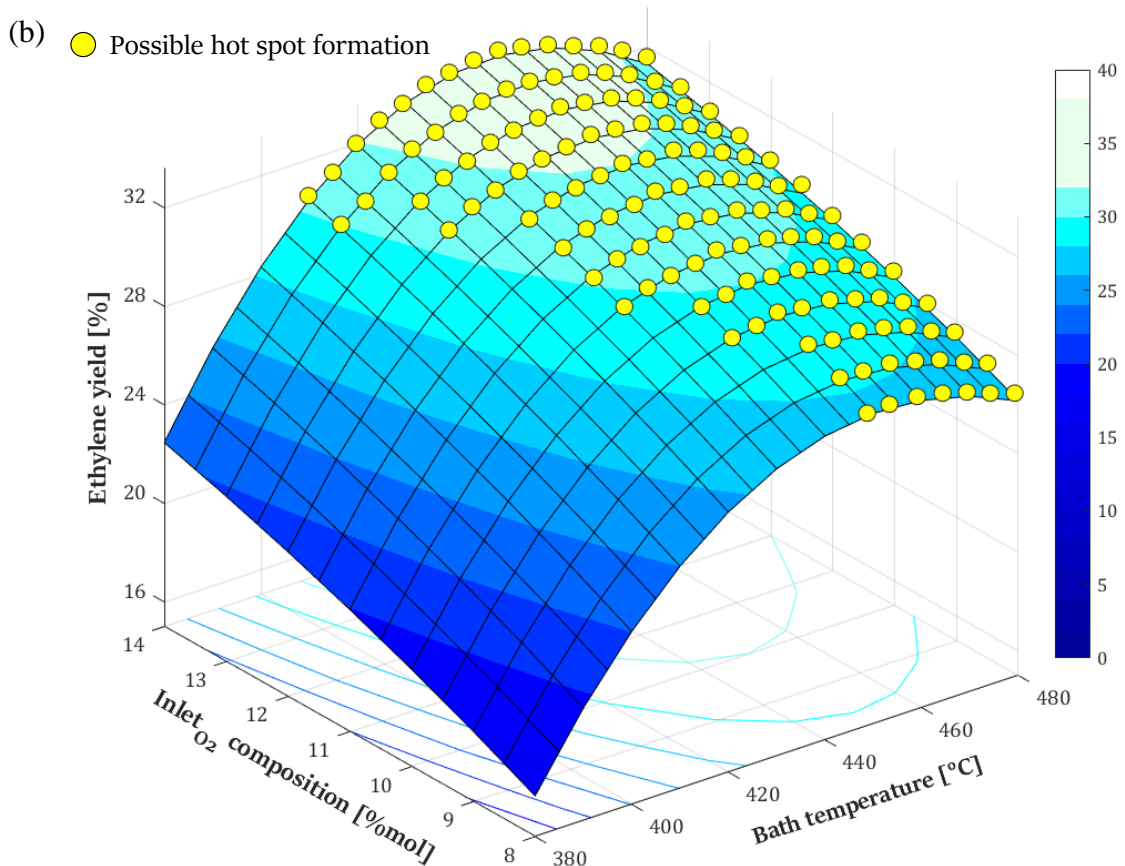
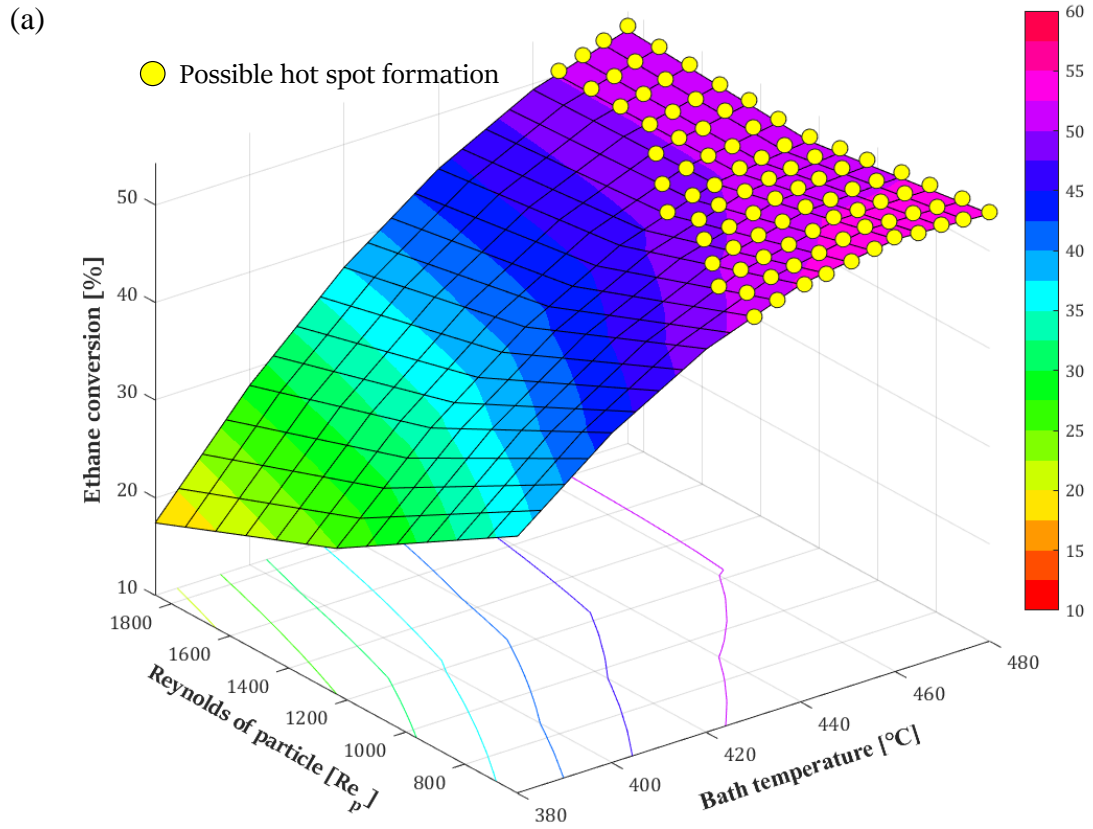


Figure 11 Effect of the coolant temperature and inlet oxygen composition on the a) ethane conversion and b) ethylene yield at the reactor outlet. % mol_{C₂H₆in}=8%, and $d_t/d_p=3.48 m_r m_s^{-1}$ and $Re_p=1240$.

Finally, [Figure 12](#) presents the effect of the coolant temperature and the particle Re_p on the ethane conversion and ethylene yield. A lower inlet flow rate results in a higher residence time in the packed bed reactor, which in combination with a higher temperature leads to a higher ethane conversion, see [Figure 12a](#). In a “hot spot safe” zone, a maximum ethylene yield from 28 to 31% is obtained for a Re_p between 620 and 1000 and coolant temperature from 410 to 440 °C ([Figure 12b](#)). As previously observed, higher coolant temperatures give rise to an increase in the ethane conversion which is mainly attributed to more pronounced oxidation reactions, as evidenced from [Figure 12a](#) and the discussion on the effect of the

coolant temperature on the product spectrum in § 3.4.1.



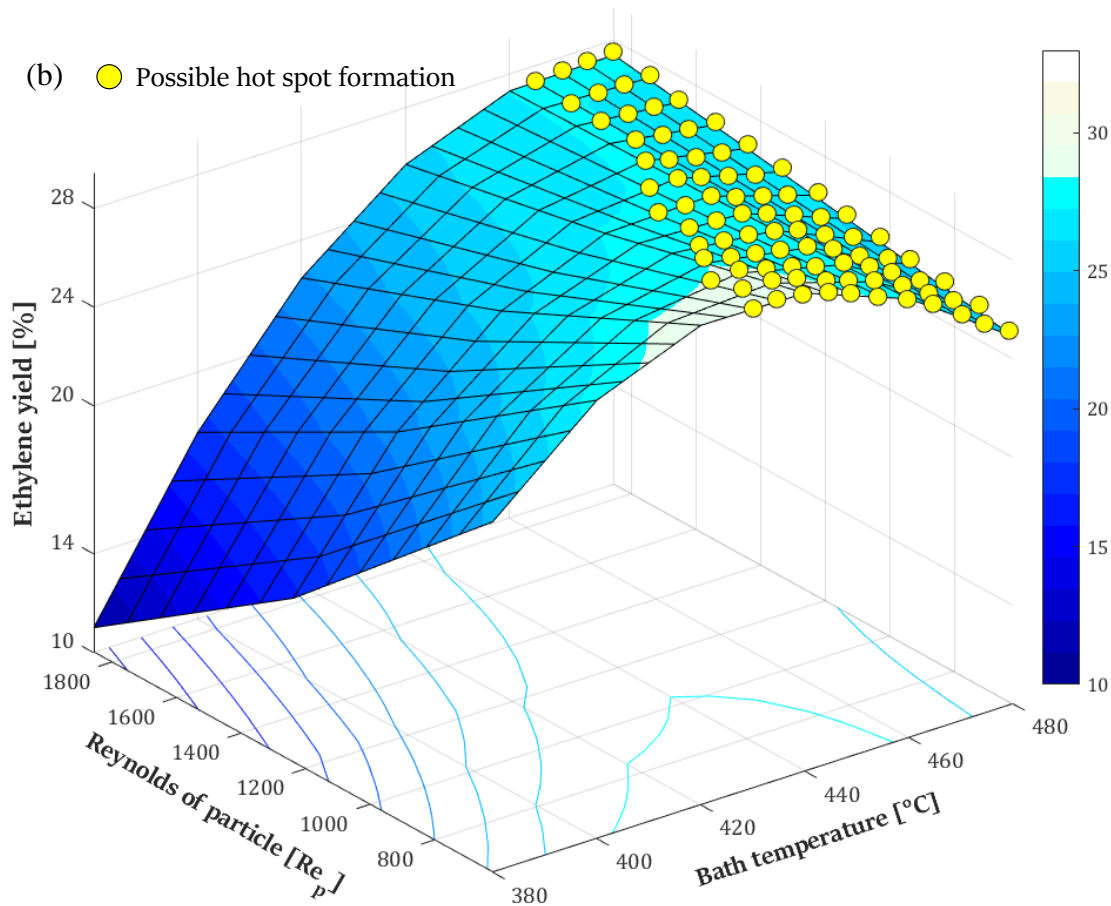


Figure 11 Effect of the coolant temperature and inlet oxygen composition on the a) ethane conversion and b) ethylene yield at the reactor outlet. $C_2H_6/O_2/N_2 = 8/8/84$, and $d_t/d_p = 3.048 m_r m_s^{-1}$.

In summary, this section shows that different operating configurations could lead the same performance. To ensure an optimal and safe operation, combinations of operating conditions that would result in the formation of a hot spot should be avoided. In this regard, the overall sensitivity analysis identified coolant temperatures ranging from 410 to 440 $^{\circ}C$, inlet concentrations of ethane from 2 to 4 %mol, inlet concentrations of oxygen from 10 to 14 %mol and Re_p from 620 to 1000 as safe operating conditions yielding the best performance of ODH- C_2 over a SnO_2 -NiO catalyst.

4. Conclusions and final remarks

A rigorous micro- and macro-scale investigation for ethylene production *via* ethane oxidative dehydrogenation was developed following a detailed modelling and simulation approach. A pseudo-heterogeneous 2D model was adopted to describe the operation of a wall-cooled industrial catalytic packed bed reactor with d_t/d_p below 10, taking into account fluid dynamics. The regime analysis and the microscopic examination of the transport phenomena revealed that radial mass and heat transport, interphase transfer, and convective mechanisms significantly contribute to the overall performance, allowing axial dispersion and conduction to be safely eliminated from the model without compromising accuracy, and reducing the run time by at least 50%. Simulations also showed that accounting for fluid dynamics is essential to properly simulate low d_t/d_p packed-bed reactors, as interstitial velocities can be up to 2.7 times larger than plug flow velocity in zones with large void fractions, resulting in lower hot spot temperatures compared to the plug flow approach. A sensitivity analysis indicated that the coolant temperature is the key operating variable affecting gas and solid phase temperatures, ethane conversion, and ethylene yield. Medium coolant temperatures are best as too low or too high temperatures will lead to insufficient conversion or overly pronounced hot spot with enhanced selectivity towards total oxidation. For instance, coolant temperatures above 440 °C led to pronounced hot spots temperatures and selectivities to CO₂ exceeding 55 %, which could damage the SnO₂-NiO catalyst structure. Inlet reactant concentrations and total molar flow rates were also found to affect product spectrum, with more severe conditions and longer residence times leading to higher reactant conversions and hot spot temperatures (hot spots up to 27 °C were identified).

Therefore, to accurately predict packed-bed reactor performance, including magnitude and position of hot spots, a detailed model is required, as omitting phenomena without prior analysis may lead to misprediction or overestimation of hot spot temperatures - an essential factor when operating at an industrial level. Finally, it was demonstrated that the operating window that leads to the highest ethylene yields is broad, yet, with an adequate prediction of the hot spot zone, it is possible to discern between the different configurations, and thus, provide insights into the safe operating window leading to optimum ethylene yield.

Acknowledgments

- Special Research Fund (BOF) - Doctoral grants for candidates from developing countries.
- CONACYT for providing a postgraduate fellowship.

Supporting information is available free of charge via the Internet at <http://pubs.acs.org/>.

References

- (1) Gärtner, C. A.; van Veen, A. C.; Lercher, J. A. Oxidative Dehydrogenation of Ethane: Common Principles and Mechanistic Aspects. *ChemCatChem* **2013**, *5* (11), 3196–3217. <https://doi.org/10.1002/cctc.201200966>.
- (2) Heracleous, E.; Lemonidou, A. A. Ni-Nb-O Mixed Oxides as Highly Active and Selective Catalysts for Ethene Production via Ethane Oxidative Dehydrogenation. Part II: Mechanistic Aspects and Kinetic Modeling. *J. Catal.* **2006**, *237* (1), 175–189. <https://doi.org/10.1016/j.jcat.2005.11.003>.
- (3) Solsona, B.; Concepción, P.; Demicol, B.; Hernández, S.; Delgado, J. J.; Calvino, J. J.; Nieto, J. M. L. Selective Oxidative Dehydrogenation of Ethane over SnO₂-Promoted NiO Catalysts. *J. Catal.* **2012**, *295*, 104–114. <https://doi.org/10.1016/j.jcat.2012.07.028>.
- (4) Zhu, H.; Rosenfeld, D. C.; Harb, M.; Anjum, D. H.; Hedhili, M. N.; Ould-Chikh, S.; Basset, J. Ni-M-O (M = Sn, Ti, W) Catalysts Prepared by a Dry Mixing Method for Oxidative Dehydrogenation of Ethane. *ACS Catal.* **2016**, *6* (5), 2852–2866. <https://doi.org/10.1021/acscatal.6b00044>.
- (5) Donaubauer, P. J.; Melzer, D. M.; Wanninger, K.; Mestl, G.; Sanchez-Sanchez, M.; Lercher, J. A.; Hinrichsen, O. Intrinsic Kinetic Model for Oxidative Dehydrogenation of Ethane over MoVTeNb Mixed Metal Oxides: A Mechanistic Approach. *Chem. Eng. J.* **2020**, *383*, 123195. <https://doi.org/10.1016/j.cej.2019.123195>.
- (6) Najari, S.; Saeidi, S.; Concepcion, P.; Dionysiou, D. D.; Bhargava, S. K.; Lee, A. F.; Wilson, K. Oxidative Dehydrogenation of Ethane: Catalytic and Mechanistic Aspects and Future Trends. *Chem. Soc. Rev.* **2021**, *50* (7), 4564–4605. <https://doi.org/10.1039/D0CS01518K>.
- (7) Botella, P.; García-González, E.; Dejoz, A.; López Nieto, J. M.; Vázquez, M. I.; González-Calbet, J. Selective Oxidative Dehydrogenation of Ethane on MoVTeNbO Mixed Metal Oxide Catalysts. *J. Catal.* **2004**, *225* (2), 428–438. <https://doi.org/10.1016/j.jcat.2004.04.024>.
- (8) Valente, J. S.; Quintana-Solórzano, R.; Armendáriz-Herrera, H.; Barragán-Rodríguez, G.; López-Nieto, J. M. Kinetic Study of Oxidative Dehydrogenation of Ethane over MoVTeNb Mixed-Oxide Catalyst. *Ind. Eng. Chem. Res.* **2014**, *53* (5), 1775–1786. <https://doi.org/10.1021/ie402447h>.
- (9) Aparicio-Mauricio, G.; Ruiz, R. S.; López-Isunza, F.; Castillo-Araiza, C. O. A Simple Approach to Describe Hydrodynamics and Its Effect on Heat and Mass Transport in an Industrial Wall-Cooled Fixed Bed Catalytic Reactor: ODH of Ethane on a MoVNbTeO Formulation. *Chem. Eng. J.* **2017**, *321*, 584–599. <https://doi.org/10.1016/j.cej.2017.03.043>.
- (10) Che-Galicia, G.; Quintana-Solórzano, R.; Ruiz-Martínez, R. S.; Valente, J. S.; Castillo-Araiza, C. O. Kinetic Modeling of the Oxidative Dehydrogenation of Ethane to Ethylene over a MoVTeNbO Catalytic System. *Chem. Eng. J.* **2014**, *252*, 75–88. <https://doi.org/10.1016/j.cej.2014.04.042>.
- (11) Moreno-Barrueta, E.; Alvarado-Camacho, C.; Durán-Pérez, J. F.; Morales-Pérez, A. A.; Castillo, C. O. On the Dynamics of the Catalytic Surface of a Bimetallic Mixed-Oxide Formulation during the Oxidative Dehydrogenation of Ethane. *Catal. Today* **2021**, No. June. <https://doi.org/10.1016/j.cattod.2021.07.028>.
- (12) Delgado, D.; Solsona, B.; Ykrelef, A.; Rodríguez-Gómez, A.; Caballero, A.; Rodríguez-Aguado, E.; Rodríguez-Castellón, E.; López Nieto, J. M. Redox and Catalytic Properties of Promoted NiO Catalysts for the Oxidative Dehydrogenation of Ethane. *J. Phys. Chem. C* **2017**, *121* (45), 25132–25142. <https://doi.org/10.1021/acs.jpcc.7b07066>.

- (13) Solsona, B.; López Nieto, J. M.; Agouram, S.; Soriano, M. D.; Dejoz, A.; Vázquez, M. I.; Concepción, P. Optimizing Both Catalyst Preparation and Catalytic Behaviour for the Oxidative Dehydrogenation of Ethane of Ni–Sn–O Catalysts. *Top. Catal.* **2016**, *59* (17–18), 1564–1572. <https://doi.org/10.1007/s11244-016-0674-z>.
- (14) Melzer, D.; Mestl, G.; Wanninger, K.; Zhu, Y.; Browning, N. D.; Sanchez-Sanchez, M.; Lercher, J. A. Design and Synthesis of Highly Active MoVTeNb-Oxides for Ethane Oxidative Dehydrogenation. *Nat. Commun.* **2019**, *10* (1), 1–9. <https://doi.org/10.1038/s41467-019-11940-0>.
- (15) Valente, J. S.; Armendáriz-Herrera, H.; Quintana-Solórzano, R.; Del Ángel, P.; Nava, N.; Massó, A.; López Nieto, J. M. Chemical, Structural, and Morphological Changes of a MoVTeNb Catalyst during Oxidative Dehydrogenation of Ethane. *ACS Catal.* **2014**, *4* (5), 1292–1301. <https://doi.org/10.1021/cs500143j>.
- (16) Annamalai, L.; Liu, Y.; Ezenwa, S.; Dang, Y.; Suib, S. L.; Deshlahra, P. Influence of Tight Confinement on Selective Oxidative Dehydrogenation of Ethane on MoVTeNb Mixed Oxides. *ACS Catal.* **2018**, *8* (8), 7051–7067. <https://doi.org/10.1021/acscatal.8b01586>.
- (17) Al-Sherehy, F. A.; Adris, A. M.; Soliman, M. A.; Hughes, R. Avoidance of Flammability and Temperature Runaway during Oxidative Dehydrogenation Using a Distributed Feed. *Chem. Eng. Sci.* **1998**, *53* (23), 3965–3976. [https://doi.org/10.1016/S0009-2509\(98\)00200-0](https://doi.org/10.1016/S0009-2509(98)00200-0).
- (18) Che-Galicia, G.; López-Isunza, F.; Corona-Jiménez, E.; Castillo-Araiza, C. O. The Role of Kinetics and Heat Transfer on the Performance of an Industrial Wall-cooled Packed-bed Reactor: Oxidative Dehydrogenation of Ethane. *AIChE J.* **2020**, *66* (4). <https://doi.org/10.1002/aic.16900>.
- (19) Rodríguez, M. L.; Ardisson, D. E.; López, E.; Pedernera, M. N.; Borio, D. O. Reactor Designs for Ethylene Production via Ethane Oxidative Dehydrogenation: Comparison of Performance. *Ind. Eng. Chem. Res.* **2011**, *50* (5), 2690–2697. <https://doi.org/10.1021/ie100738q>.
- (20) Rodriguez, M. L.; Ardisson, D. E.; Lemonidou, A. A.; Heracleous, E.; López, E.; Pedernera, M. N.; Borio, D. O. Simulation of a Membrane Reactor for the Catalytic Oxidehydrogenation of Ethane. *Ind. Eng. Chem. Res.* **2009**, *48* (3), 1090–1095. <https://doi.org/10.1021/ie800564v>.
- (21) Hamel, C.; Tóta, Á.; Klose, F.; Tsotsas, E.; Seidel-Morgenstern, A. Analysis of Single and Multi-Stage Membrane Reactors for the Oxidation of Short-Chain Alkanes - Simulation Study and Pilot Scale Experiments. *Chem. Eng. Res. Des.* **2008**, *86* (7), 753–764. <https://doi.org/10.1016/j.cherd.2008.03.025>.
- (22) Fattahi, M.; Kazemeini, M.; Khorasheh, F.; Darvishi, A.; Rashidi, A. M. Fixed-Bed Multi-Tubular Reactors for Oxidative Dehydrogenation in Ethylene Process. *Chem. Eng. Technol.* **2013**, *36* (10), 1691–1700. <https://doi.org/10.1002/ceat.201300148>.
- (23) Che-Galicia, G.; Ruiz-Martínez, R. S.; Rios-Morales, D.; Ayala-Romero, J. A.; Castillo-Araiza, C. O. Kinetic and Reactor Performance of a Ni-Based Catalyst during the Production of Ethene. *Chem. Eng. Commun.* **2018**, *205* (3), 372–386. <https://doi.org/10.1080/00986445.2017.1396538>.
- (24) López, E.; Heracleous, E.; Lemonidou, A. A.; Borio, D. O. Study of a Multitubular Fixed-Bed Reactor for Ethylene Production via Ethane Oxidative Dehydrogenation. *Chem. Eng. J.* **2008**, *145* (2), 308–315. <https://doi.org/10.1016/j.cej.2008.08.029>.
- (25) Che-galicia, G.; Ruiz-martínez, R. S.; López-isunza, F.; Castillo-araiza, C. O. Modeling of Oxidative Dehydrogenation of Ethane to Ethylene on a MoVTeNbO / TiO₂ Catalyst in an Industrial-Scale Packed Bed

- Catalytic Reactor. *Chem. Eng. J.* **2015**, *280*, 682–694. <https://doi.org/10.1016/j.cej.2015.05.128>.
- (26) Skoufa, Z.; Giannakakis, G.; Heracleous, E.; Lemonidou, A. A. Simulation-Aided Effective Design of a Catalytic Reactor for Ethane Oxidative Dehydrogenation over NiNbOx. *Catal. Today* **2018**, *299*, 102–111. <https://doi.org/10.1016/j.cattod.2017.03.004>.
- (27) Castillo-Araiza, C. O.; López-Isunza, F. Modeling the Partial Oxidation of O-Xylene in an Industrial Packed-Bed Catalytic Reactor: The Role of Hydrodynamics and Catalyst Activity in the Heat Transport. *Ind. Eng. Chem. Res.* **2010**, *49* (15), 6845–6853. <https://doi.org/10.1021/ie901720z>.
- (28) Castillo-Araiza, C. O.; López-Isunza, F. The Role of Catalyst Activity on the Steady State and Transient Behavior of an Industrial-Scale Fixed Bed Catalytic Reactor for the Partial Oxidation of o-Xylene on V2O5/TiO2 Catalysts. *Chem. Eng. J.* **2011**, *176–177*, 26–32. <https://doi.org/10.1016/j.cej.2011.06.051>.
- (29) Alvarado-Camacho, C.; Poissonnier, J.; Thybaut, J.; Castillo, C. O. Unravelling the Redox Mechanism and Kinetics of a Highly Active and Selective Ni-Based Material during the Oxidative Dehydrogenation of Ethane. *React. Chem. Eng.* **2021**. <https://doi.org/10.1039/D1RE00275A>.
- (30) Finlayson, B. A. *Nonlinear Analysis in Chemical Engineering*; 1980.
- (31) 2 Runge-Kutta and Allied Single-Step Methods. In *Numerical Solution of Ordinary Differential Equations*; Lapidus, L., Seinfeld, J. H., Eds.; Mathematics in Science and Engineering; Elsevier, 1971; Vol. 74, pp 39–106. [https://doi.org/https://doi.org/10.1016/S0076-5392\(08\)63009-X](https://doi.org/https://doi.org/10.1016/S0076-5392(08)63009-X).
- (32) Li, S. *Residence Time Distribution and Flow Models for Reactors*; 2017. <https://doi.org/10.1016/b978-0-12-410416-7.00005-7>.
- (33) Iordanidis, A. A. *Mathematical Modeling of Catalytic Fixed Bed Reactors*, University of Twente, 2002.
- (34) Bird, R. B.; Stewart, W. E.; Lightfoot, E. N. *Transport Phenomena*; J. Wiley, 2002.
- (35) Anastasov, A. I. A Study of the Influence of the Operating Parameters on the Temperature of the Hot Spot in a Fixed Bed Reactor. *Chem. Eng. J.* **2002**, *86*, 287–297. [https://doi.org/10.1016/S1385-8947\(01\)00178-4](https://doi.org/10.1016/S1385-8947(01)00178-4).

Table of Contents graphic

